Article

Two Classes of Gamma-Ray Bursts Distinguished within the First Second of their Prompt Emission

Lána Salmon [1]*, Lorraine Hanlon [1] and Antonio Martin-Carrillo [1]

[1] School of Physics and Centre for Space Research, University College Dublin, Belfield, Dublin 4,D04 V1W8, Ireland; lana.salmon@ucdconnect.ie
* Correspondence: lana.salmon@ucdconnect.ie

Abstract: Studies of Gamma-Ray Burst (GRB) properties, such as duration and spectral hardness, have found evidence for additional classes, beyond the short/hard and long/soft prototypes using model-dependent methods. In this paper, a model-independent approach has been used to analyse the gamma-ray light curves of large samples of GRBs detected by BATSE, *Swift*/BAT and *Fermi*/GBM. All the features are extracted from the GRB time profiles in 4 energy bands using the Stationary Wavelet Transform and Principal Component Analysis. t-distributed Stochastic Neighbourhood Embedding (t-SNE) visualisation of the features reveal two distinct groups of *Swift*/BAT bursts using the T_{100} interval with 64 ms resolution data. When the same analysis is applied to 4 ms resolution data, 2 groups are seen to emerge within the first second (T_1) post-trigger. These two groups consist primarily of short/hard (Group 1) and long/soft (Group 2) bursts, and are 95% consistent with the groups identified using the T_{100} 64 ms resolution data. Kilonova candidates, arising from compact object mergers, are found to belong to Group 1, while those events with associated supernovae fall into Group 2. Differences in cumulative counts between the two groups in the first second, and in the minimum variability timescale, identifiable only with the 4 ms resolution data, may account for this result. Short GRBs have particular significance for multi-messenger science as a distinctive EM signature of a binary merger which may be discovered from its gravitational wave emission. Incorporating the T_1 interval into classification algorithms may support rapid classification of GRBs, allowing improved prioritisation of targets for follow-up observations.

Keywords: gamma-ray burst; feature extraction; machine learning

Citation: Lastname, F.; Lastname, F.; Lastname, F. Title. *Preprints* **2022**, *1*, 0. https://doi.org/

1. Introduction

Gamma-Ray Bursts (GRBs) are traditionally classified based on their duration and hardness as short/hard or long/soft bursts. These classes are separated at $T_{90} \approx 2$ s, derived from the duration distribution of the Third BATSE catalogue [1]. T_{90} is defined as the duration during which 5–95% of the counts above background are detected. The properties of these classes suggest different progenitors – long GRBs often lie in star forming galaxies [2] and some long GRBs are associated with Type Ic supernovae [3–6] therefore linking them to the deaths of massive stars [7]. Short GRBs are linked to compact object mergers [8,9] as some short GRBs have been identified near elliptical galaxies [10], and many are offset from their hosts [11,12]. The detection of GRB 170817A [13,14] associated with the neutron star merger GW170817, detected in gravitational waves by LIGO [15], lends further weight to this progenitor theory.

Classification of GRBs based on their duration is affected by the significant overlap between the duration distributions of the long and short groups and is further complicated by a possible 'intermediate' class of GRBs, first identified through Gaussian fits to the duration distribution of GRBs in the Third BATSE catalogue [16]. Clustering of the duration-hardness plane, and multi-dimensional analyses of GRB samples from different satellites, have also revealed evidence for more than two classes of bursts.

Salmon *et al.* [17] presents a review of previous studies and reports on an updated clustering analysis of *Swift*/BAT and *Fermi*/GBM bursts which finds that Gaussian models applied to *Swift*/BAT and *Fermi*/GBM GRB samples recover three clusters, including

an intermediate duration one. However, the latter is identified as an excess Gaussian component when an entropy criterion is used and the resulting best-fit solution contains two classes, broadly consistent with the typical short and long duration groups. A key conclusion of the analysis is that model-based methods may identify spurious components in one-, two- and multi-dimensional analyses of GRB samples and that model-independent analyses of GRBs should be conducted, for example using GRB light curves.

Short GRBs with extended emission have been detected, which may form an additional sub-class [18–20] and are possibly associated with a magnetar central engine [21]. These episodes, combined with late X-ray flares in some short GRBs, and the non-detection of supernovae associated with some long GRBs, led to the suggestion of a new classification scheme by Zhang *et al.* [22]. Type I (massive star/collapsar origin) and Type II (compact-object merger origin) bursts are defined by multiple observational criteria beyond duration and hardness [23]. Other classification methods based on afterglow and host galaxy properties [24], minimum variability timescales [25] and prompt emission and energetics have been defined [26–30]. The instrument, sample size and classification method used can lead to different results [31], and the collapsar/merger fractions for each instrument's sample cannot simply be defined by a T_{90}=2 s threshold [32].

Analysis of GRB light curves in several bands does not rely on summary statistics, such as parameters derived from spectral fits which could be poorly fit or incorrect. Jespersen *et al.* [33] extracted features from 64 ms resolution *Swift*/BAT light curves using Discrete Fourier Transforms and found two groups using t-distributed Stochastic Neighbourhood Embedding (t-SNE). This approach does not assume the underlying distribution of the variables, unlike model-based clustering and distribution fitting.

An alternative to Fourier analysis is wavelet analysis, which has been used to study non-stationary time-series [34]. Wavelet analysis has the advantage of extracting both frequency and temporal information and for this reason it has been used to compress and de-noise GRB light curves for the study of their time evolution [35–37], to identify peaks [38–41], and to quantify the minimum variability timescale of GRBs [42–46]. Wavelet decomposition has been used to reduce the dimensionality of supernova light curves for classification [47], and has been combined with Principal Component Analysis (PCA) and t-SNE for classification [48,49]. Lochner *et al.* [48] found that classifiers performed better when supplied with wavelet coefficients of supernova light curves, in contrast to feature extraction using parametric models.

GRB pulses exhibit spectral evolution, including hard-to-soft [50] or intensity-tracking [51] behaviour. Other common features of all GRB pulses include longer observed durations at lower energies [52] and asymmetric shapes [53,54]. These commonalities suggest that a similar emission mechanism creates GRB pulses, regardless of the progenitor [55,56].

However, pulses in short and long bursts also exhibit some differences. Long GRB pulses are observed to peak earlier at higher energies, but these spectral lags are not typically significant in short GRBs [18,54,57–63]. The minimum variability timescales [44–46] retrieved from wavelet analysis of long and short GRBs are $\sim$ 200 ms and $\sim$ 10 ms respectively. Hakkila and Preece [64] found that pulses in short GRBs are shorter and harder than long GRBs, and exhibit more spectral evolution. Coupled with the observation that shorter pulses have higher peak flux and $\sim$ 90% of short GRBs consist of a single pulse, compared to 25–40% for long GRBs, pulse properties are likely to be a distinguishing feature in the first seconds of a burst. In particular, spectral evolution is evident at early times in previous studies of bursts from BATSE [65–70], *Swift* [71] and *Fermi*/GBM [72–74].

Redshift effects have not been observed in GRB light curves as standard time dilation of GRB pulses is thought to be masked by a contrasting effect whereby only the shorter, brightest portion of the burst is observed [75]. Therefore, analysis of GRB light curves is unlikely to be strongly affected by cosmological effects [76].

In this work, the light curves of GRBs in 4 energy bands from 3 different instruments are analysed using wavelets as a feature extraction method. The T_{100} burst intervals, during which 100% of the counts above background are recorded, are studied at 64 ms

resolution and the early phase of GRB emission (first few seconds) at 4 ms resolution. Wavelet coefficients are extracted and reduced and then visualised using PCA and t-SNE. Section 2 outlines the sample construction, while Section 3 provides details of the methods applied to perform feature extraction. Results are presented in Section 4 and consistency checks with other studies and between instrument samples are discussed in Section 5. The classification of notable GRBs is presented in Section 6. Possible signatures in the first second are discussed in Section 7 while conclusions are outlined in Section 8.

2. GRB Light Curves

The GRB samples analysed include bursts detected by the BATSE instrument on the *Compton Gamma-Ray Observatory* [77], the Burst Alert Telescope (BAT) on the *Neil Gehrels Swift Observatory* (hereafter *Swift*/BAT; Gehrels *et al.* 78) and the Gamma-ray Burst Monitor (GBM) on the *Fermi Gamma-ray Space Telescope* (hereafter *Fermi*/GBM; Meegan *et al.* 79).

2.1. BATSE

The BATSE 64 ms-binned light curves are stored as ascii files on the BATSE Public Data Archive (https://heasarc.gsfc.nasa.gov/FTP/compton/data/batse/trigger/, accessed on 17/02/21). There are 2704 bursts in the final BATSE catalogue from April 21 1991 – August 17 2000, and 1956 light curves at 64 ms resolution were available. Background subtraction is applied via polynomial fits to the 64 ms light curves pre- and post-burst. The BATSE 4 ms-binned light curves were generated using the TTE files for individual bursts in the BATSE Public Data Archive, which stores 1732 TTE files, 1721 of which have successful background subtraction. The count rate is divided by the number of triggered detectors to obtain light curves measured in counts s^{-1} det^{-1}. The resulting light curves are stored in the 4 standard BATSE bands (20–50 keV, 50–100 keV, 100–300 keV and >300 keV).

2.2. Swift/BAT

The *Swift*/BAT Gamma-Ray Burst Catalogue (https://swift.gsfc.nasa.gov/results/batgrbcat/, accessed on 29/01/21) hosts ascii files containing the 64 ms- and 4 ms-binned background-subtracted light curves. There are 1388 GRBs detected between December 17 2004 – August 28 2020 in this catalogue which is extended from the Third *Swift* BAT Catalogue [80]. 1273 light curve files are available at 4 ms resolution, containing 4 background subtracted light curves, corresponding to 4 bands (15–25 keV, 25–50 keV, 50–100 keV and 100–350 keV) in units of counts s^{-1} det^{-1}. 22 bursts with no documented duration (T_{90}) are removed from the sample. At 64 ms resolution, light curves are available for the same set of bursts, with three additional GRBs added to the sample.

2.3. Fermi/GBM

Fermi/GBM light curves were generated from TTE data in 64 ms and 4 ms bins using the *Fermi*-GBM Data Tools [81]. 3000 bursts from August 10 2008 – March 17 2021 are included, with 2678 successful background subtracted light curves created. Only triggered detectors are used, and the background intervals defined in the *Fermi*/GBM catalogue are used for background subtraction. Count rates are transformed to counts s^{-1} det^{-1} by normalising by the number of triggered detectors. Unlike *Swift* and BATSE, *Fermi*/GBM does not have defined light curve bands. Thus, they are chosen to capture the energy ranges of the NaI and BGO detectors, and the bands considered in hardness ratio calculations. Four energy bands are considered: the *Fermi* trigger band (50–300 keV), the lower energy band used in hardness ratio calculations (8–50 keV), the energy range of the NaI detectors (8–1000 keV) and higher energy range of the BGO detectors (> 1000 keV). The effect of the choice of these bands was studied by repeating the analysis on light curves within the four *Swift* bands, which was shown to produce similar results.

3. Feature Extraction

The feature extraction algorithm consists of multiple steps, which are outlined in Figure 1 for the analysis of light curves in the T_{100} interval at 64 ms resolution. Light curves are first pre-processed before the Stationary Wavelet Transform is applied. PCA is used to reduce the dimensionality of the resulting coefficients before being visualised with a t-SNE map. Figure 2 depicts the steps followed for the analysis of the first second of prompt emission. This section outlines the details of each step in the feature extraction algorithm.

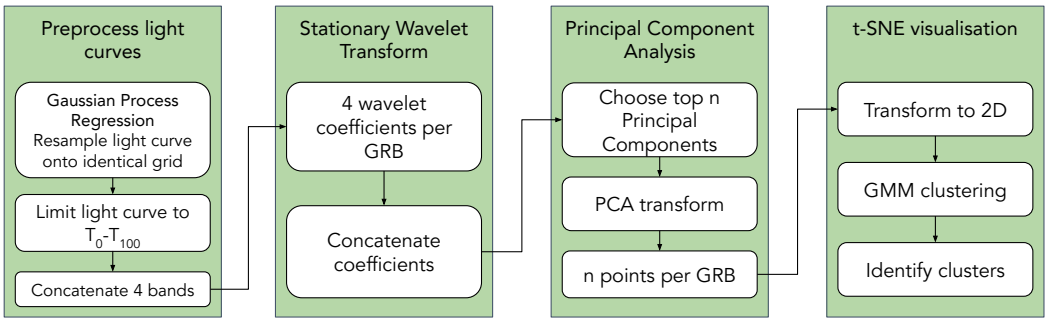

Figure 1. Flowchart of the feature extraction and clustering algorithm for analysis of 64 ms binned light curves in the interval T_0 to T_{100}.

3.1. Light Curve Pre-processing

3.1.1. 64 ms Light Curves

To obtain counts recorded at identical times relative to the trigger time for each light curve, BATSE and *Swift*/BAT light curves are modelled and resampled onto an identical grid using Gaussian Process Regression (GPR), a machine learning method that uses the input data to infer the function to explain the observations [82]. Gaussian processes model observations as joint multivariate normal distributions, which can be fully specified by a mean function and covariance matrix. GPR determines the mean function and the entries of the covariance matrix using a user specified covariance function (kernel). Hyperparameters of the kernel are optimised to maximise the marginal likelihood of the data under the Gaussian process prior.

The Gaussian Process model is implemented using the GPFlow library in Python [83], which originates from GPy but is built on TensorFlow [84]. A heteroscedastic regression model is used, which incorporates uncertainty on each point into the interpolation process by applying less weight to points with greater uncertainty. The radial-basis function kernel (also known as squared exponential kernel) is used as it is infinitely differentiable and produces smooth functions. The Adam and natural gradient optimisers are used to converge to the best-fit hyperparameters. The resulting equally-spaced, evenly-sampled 64 ms light curves are zero-padded beyond T_{100} to ensure noise is discarded. The T_{100} interval is extracted from the GRB catalogues. The four-band light curves are concatenated together for input to the feature extraction algorithm depicted in Figure 1.

3.1.2. 4 ms Light Curves

Wavelet decomposition requires time series of equal and even lengths. At 4 ms resolution, the light curves are restricted to even-length time intervals starting at T_0, the burst start time documented in the GRB catalogues. Light curves spanning different intervals are created, and extended in intervals of 0.1 s until T_0+3 s. Many of the BATSE TTE datasets do not extend past 3 s, and BATSE light curves are zero padded if they do not extend to the specified interval. For each GRB, the light curves in the four energy bands are concatenated together to form one vector for input to the feature extraction algorithm, depicted in Figure 2 for the case in which light curves between T_0 and T_0+1.004s are studied.

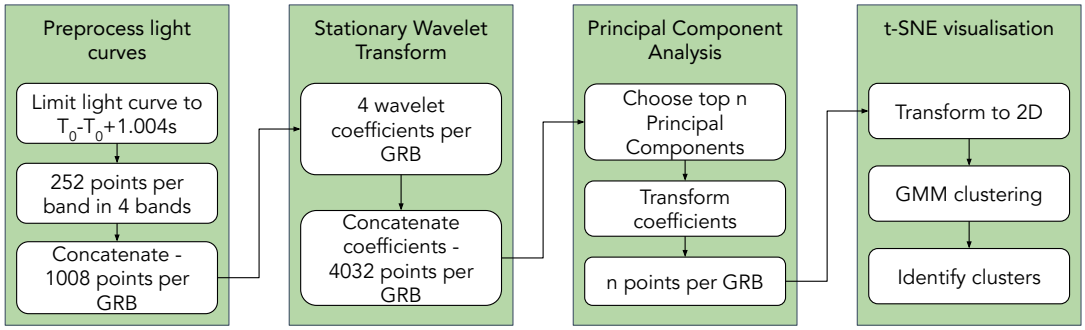

Figure 2. Flowchart of the feature extraction and clustering algorithm for analysis of light curves in the interval T_0 to T_0+1.004 s.

3.2. Wavelet Decomposition

Fourier analysis is often used to examine the frequency composition of signals and to extract features from time series (e.g. Jespersen *et al.* [33]). However, a drawback of Fourier transforms is the loss of temporal information and the stringent sine and cosine basis functions. Wavelets are more suited to the analysis of images, music and transient events as they overcome the limitations of Fourier analysis by encoding both time and frequency information in the basis function [85]. The Stationary Wavelet Transform (SWT), also known as the Á Trous algorithm [86], is a shift-invariant transform which convolves a signal with scaled and shifted versions of the basis wavelet function. The shift-invariance feature of the SWT has made it a popular method for pattern recognition [87,88]. The SWT returns two coefficients, known as Approximation and Detail coefficients, of equal length to the input signal. The coefficients are computed using a filter-bank algorithm [34] with low- and high-pass filters, which decomposes the input signal. Multiple levels of decomposition can be performed whereby the output of the low-pass filter is fed successively to the next decomposition level.

The `pywt.swt` function of the PyWavelets package [89] is applied to the light curve vectors using the symlet family of wavelets, which is a more symmetric version of the Daubechies wavelet family [90], but other wavelet families produce similar results. A two-level decomposition is performed, resulting in 4 components of length equal to the vector containing the light curves in four bands (Figure 2). These are concatenated into one vector for each GRB prior to dimensionality reduction.

3.3. Principal Component Analysis

After performing a two-level wavelet decomposition, the data set for each GRB has increased in length by a factor of four. A dimensionality reduction technique is used to extract only the most significant information encoded in the wavelet coefficients. PCA is a form of decomposition which extracts uncorrelated Principal Components from correlated data via an orthogonal transformation [91,92]. PCA involves eigenvalue decomposition of the covariance matrix of the input wavelet coefficient data. The eigenvectors are sorted by the magnitude of their eigenvalues. The user must choose how many eigenvectors to keep based on the percentage of variance explained by each eigenvector. The chosen eigenvectors represent the original data in a new PCA reference frame and are known as the Principal Components (PCs). The matrix of PCs is used to project the wavelet coefficients onto the lower dimensional PCA space.

In this work, PCA is carried out using the `sklearn.decomposition.PCA` function. For *Swift*/BAT, the components whose cumulative variance reaches $> 70\%$ are chosen as the new representation of the dataset, as the number of required components to meet $> 90\%$ is large. For BATSE and *Fermi*/GBM, the number of components retained ensures $>90\%$ of the variance is captured.

3.4. t-SNE

The chosen PCA components require transformation to a 2D space so that features can be visualised. Stochastic Neighbourhood Embedding (SNE; Hinton and Roweis 93) provides a 2D visual representation of the components on arbitrary axes by computing the probability that each point is a neighbour of another point. It uses a Gaussian probability density and Kullback-Leibler minimisation [94] to ensure the low-dimensional space adequately represents the high-dimensional space. A user-specified parameter called Perplexity specifies the importance of local or global structure. In general, the Perplexity can be considered as representative of the number of nearest neighbours of each point.

t-SNE (t-distributed SNE; Maaten and Hinton 95) uses a Student t-distribution with a single degree of freedom, replacing the Gaussian comparison between points. The `sklearn.manifold.TSNE` method is used with a Perplexity which maximises the separation of clusters in the final representation. In this case, the smaller *Swift*/BAT sample is analysed with a Perplexity of 40, while for the larger samples of BATSE and *Fermi*/GBM, Perplexities of 50 and 70 respectively are used. The result is a 2D representation of the PCA feature space, in which similar light curves are grouped together.

3.5. GMM Clustering

Finally, Gaussian Mixture Model-based (GMM) clustering is applied to the t-SNE plots to identify clusters using the MCLUST package in R [96,97]. GMM clustering assumes that the observed data are generated from a mixture of K components, where the density of each component is described by a multivariate Gaussian distribution. MCLUST applies 14 different models and chooses the best-fit model and number of clusters based on the Bayesian Information Criterion (BIC; Schwarz *et al.* [98]). Since the underlying distributions are non-Gaussian, clusters are combined using the `clustCombi` function to converge on the optimum number of clusters calculated via an entropy criterion [99].

4. Results

The results obtained by analysing GRB light curves as described in Section 3 for the T_{100} intervals at 64 ms resolution, and for the first three seconds post-trigger at 4 ms resolution, are presented.

4.1. 64 ms Results

The t-SNE plots, coloured by burst duration (T_{90}), are shown in Figure 3 for the T_{100} intervals of bursts from BATSE, *Swift*/BAT and *Fermi*/GBM. t-SNE plots produce a mapping onto an arbitrary space whereby the scale of the axes have no units or physical meaning. Thus, the t-SNE plots presented in this paper do not label the X and Y axes, and the precise position of points along the axes is not significant. However, structure within the t-SNE space is significant and is identified. A separate group of shorter duration bursts is evident in Figure 3b for Swift/BAT, while for BATSE and *Fermi*/GBM, the separation is not as clear.

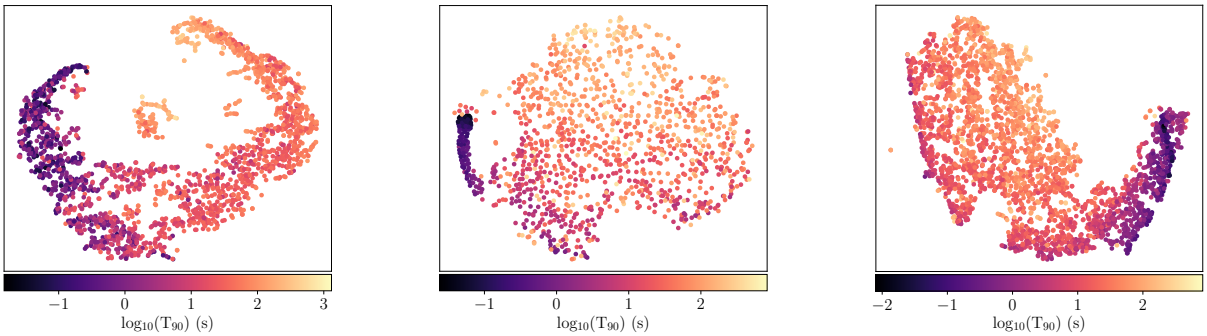

(a) BATSE **(b)** *Swift*/BAT **(c)** *Fermi*/GBM

Figure 3. 2D t-SNE representation of the extracted wavelet and PCA features from the 64 ms light curves from T_0 to T_{100}, coloured by burst duration T_{90}, for (a) BATSE, (b) *Swift*/BAT and (c) *Fermi*/GBM.

GMM clustering applied to the t-SNE map for *Swift*/BAT (Figure 3b) identifies 4 clusters of bursts. However, the distribution is complex and is likely unsuitable for model-based clustering. When coloured by duration, it is clear that there are two groups of bursts identified within the T_{100} intervals of *Swift*/BAT light curves, one consisting primarily of short bursts and a larger group of longer duration bursts.

4.2. 4 ms Results

The t-SNE plots from the analysis of the 4 ms light curves are shown in the animations in Figure 4, coloured by burst duration (T_{90}). The video animations are available to download in the Supplementary Materials. The intervals shown in each iteration of the t-SNE plot increase by 0.1 s, starting from the burst trigger time, T_0. For *Swift*/BAT, a small group of shorter duration bursts begins to form and separate from the larger group of longer bursts within T_0+0.2 s. This shorter group of bursts grows and detaches from the longer group by T_0 to T_0+1.004 s, remaining detached up to the first 3 seconds post-trigger which is the maximum interval available at 4 ms resolution. For BATSE and *Fermi*/GBM, the distinction between groups is not as clear, but a similar pattern is observed - a group of shorter bursts begins to form at $\sim T_0$+0.2 s and grows, separating itself from the larger, longer duration, group. We conclude that the time at which the two clusters of bursts become clearly separated is T_0+1.004 s.

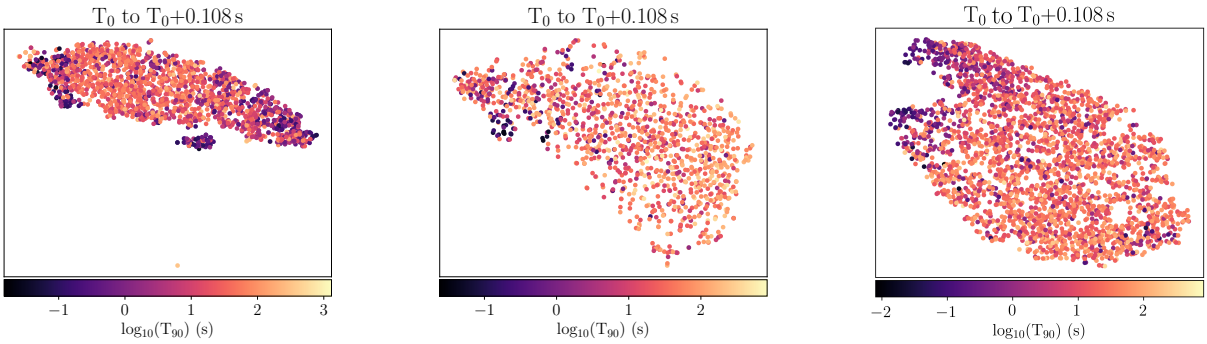

(a) BATSE **(b)** *Swift*/BAT **(c)** *Fermi*/GBM

Figure 4. Animation of t-SNE projections for different GRB light curve time intervals at 4 ms resolution for (a) BATSE (b) *Swift*/BAT and (c) *Fermi*/GBM, coloured by their T_{90} duration. The title indicated on the top axis of each figure denotes the time interval, since the burst trigger, analysed. The video files are available in the Supplementary Materials.

4.3. Properties of GRB Clusters Identified in the First Second Post-Trigger

2D t-SNE representation of the extracted wavelet and PCA features from the first second (T_0 to T_0+1.004 s) of GRB light curves, coloured by burst duration T_{90} and hardness ratio HR_{32} for BATSE, *Swift*/BAT and *Fermi*/GBM, are shown in Figure 5. The projections indicate the presence of two groups of bursts, which can be seen clearly in Figure 5b for *Swift*/BAT. For BATSE (Fig. 5a) and *Fermi*/GBM (Fig. 5c), this separation is less well-defined.

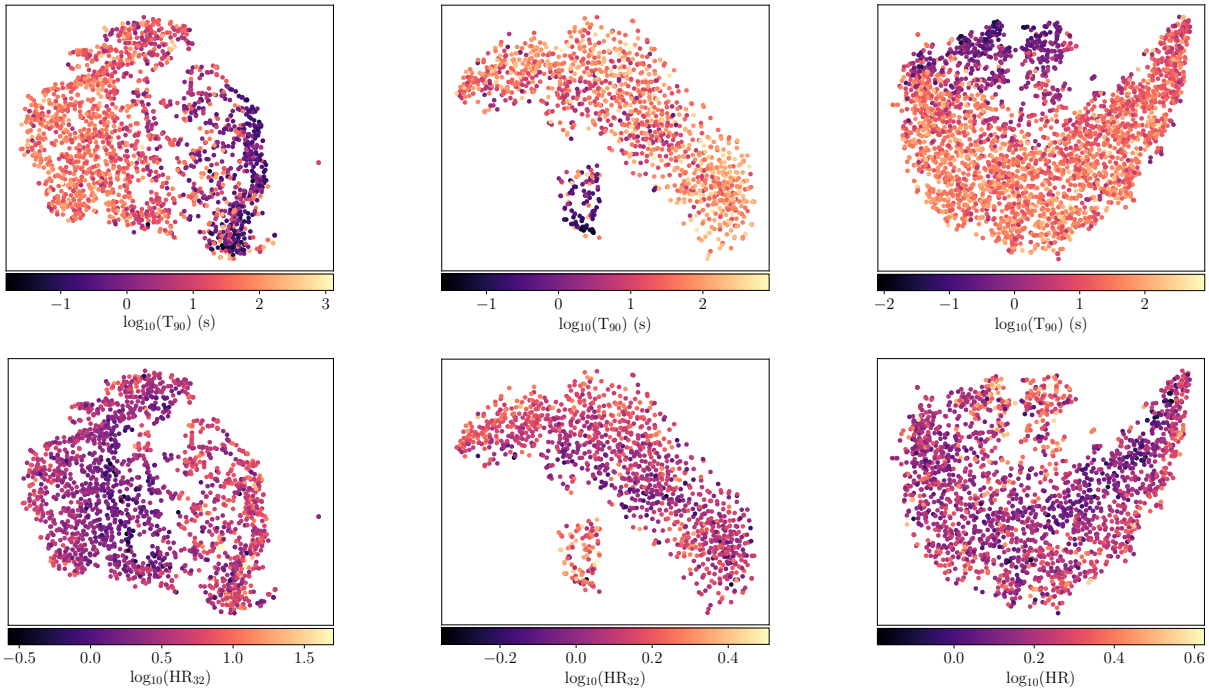

(a) BATSE **(b)** *Swift*/BAT **(c)** *Fermi*/GBM

Figure 5. 2D t-SNE representation of the extracted wavelet and PCA features from the first second (T_0 to T_0+1.004 s) of burst light curves, coloured by burst duration T_{90} (top row) and hardness ratio HR_{32} (bottom row) for (a) BATSE, (b) *Swift*/BAT and (c) *Fermi*/GBM. Hardness ratios (HR_{32}) for *Swift*/BAT and BATSE are calculated as the ratio of fluence in Band 3 and Band 2. The hardness ratio of *Fermi*/GBM bursts is defined as the ratio of fluence in the 50–300 keV and 10–50 keV bands, calculated using the best-fit spectral parameters.

GMM clustering applied to the *Swift*/BAT projection identifies two separate groups, shown in Figure 6a. The group consisting of mostly short/hard bursts is labelled Group 1, and the larger, longer duration group is denoted Group 2. The groups are shown projected onto the duration-hardness plane in Figure 6b.

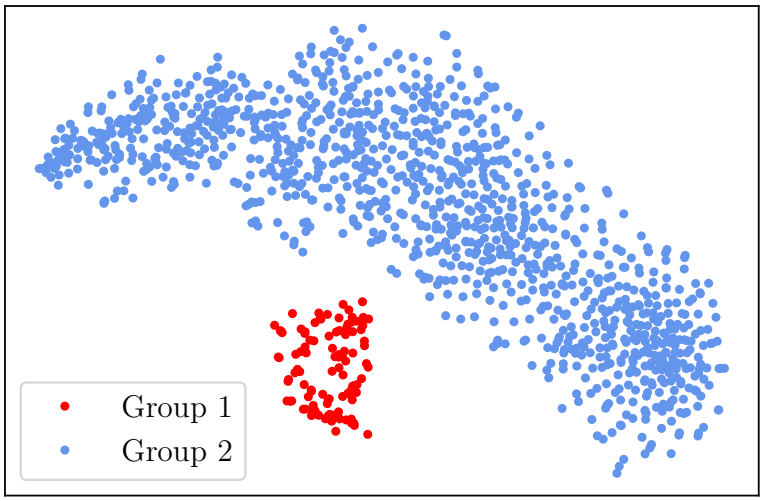

(a)

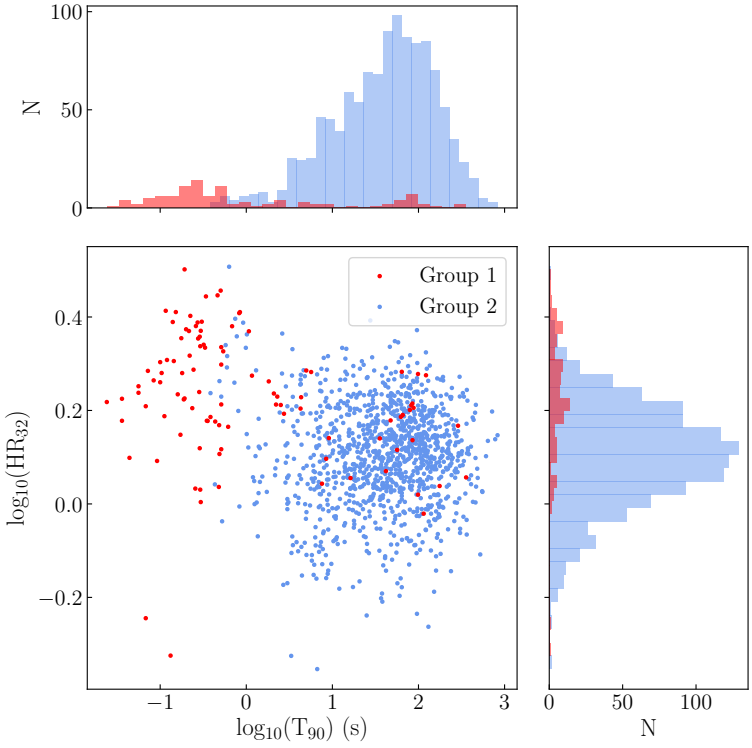

(b)

Figure 6. (a) The t-SNE map of *Swift*/BAT bursts derived from the T_0 to T_0+1.004 s interval at 4 ms resolution showing 2 clearly separated groups and (b) their projection onto the duration-hardness plane. Histograms indicate the distribution of duration and hardness for each group.

Two-dimensional Kolmogorov–Smirnov (KS) tests applied to Group 1 and Group 2 verify that there are statistically significant differences in GRB properties such as duration (T_{90}), hardness (HR_{32}), peak energy (E_{peak}) and fluence (S) of the two clusters. Table 1 presents the results of the KS test. The probability (p-value) presented in Table 1 indicates the probability that Groups 1 and 2 are drawn from the same distribution. This hypothesis is rejected, as all probabilities are below 1%. Figure 7 demonstrates the distribution of the GRB properties for Group 1 and Group 2.

Table 1. Results of the 2D KS test comparing Group 1 and Group 2 identified within the first second of prompt emission of *Swift*/BAT bursts.

Parameter	p-value
T_{90}	4.3×10^{-42}
HR_{32}	1.7×10^{-19}
E_{peak}	1.9×10^{-3}
Fluence (15-350 keV)	2.9×10^{-22}

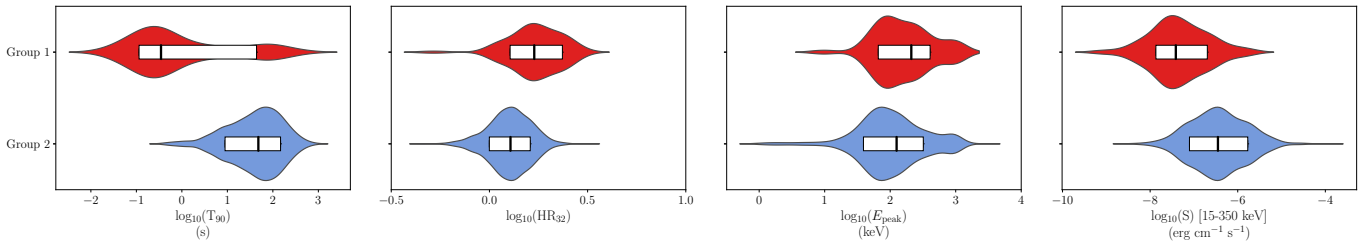

Figure 7. Violin plots showing the distribution of GRB properties for Group 1 (red) and Group 2 (blue) *Swift*/BAT bursts identified in the T_0 to T_0+1.004 s light curve interval. The white box plots represent the 1σ interval (i.e. the 16th to 84th percentile), with the median of each parameter marked as a black line.

Table 2 lists the cluster memberships of a subset of the *Swift* GRBs for both the analysis of the T_{100} interval at 64 ms resolution, and the interval from T_0 to T_0+1.004 s at 4 ms resolution. The full table is available to download from the Supplementary Materials. When the first 1 s of prompt emission is considered, Group 1 contains 107 bursts, 73 of which are short duration (T_{90} <2 s). There are 1144 bursts in Group 2, containing 1112 long duration bursts (T_{90} >2 s). The composition of each group and the properties of GRBs in Groups 1 and 2 are discussed further in Section 5.

Table 2. Group membership of *Swift* GRBs based on the analysis of the first second of prompt emission at 4 ms resolution (T_1) and the T_{100} interval at 64 ms resolution. The full table is provided in the Supplementary Materials.

GRB	T_1 Group	T_{100} Group	T_{90} (s)	HR_{32}
GRB041220	2	2	5.6	1.3
GRB041223	2	2	109.1	1.8
GRB041224	2	2	177.6	1.2
...	...	...	...	...
GRB200809B	... [1]	2	4.2	1.8
GRB200819A	2	2	26.9	1.0
GRB200829A	... [1]	2	13.1	1.9

[1] No 4 ms light curve file available.

As with the T_{100} analysis (Section 4.1), the results obtained for the T_0 to T_0+1.004 s interval at 4 ms resolution for BATSE and *Fermi*/GBM GRBs are not as clear-cut as for *Swift*/BAT. In the case of BATSE, GMM clustering with MCLUST identifies 6 clusters within the t-SNE projection in Figure 5a. However, we tentatively identify by eye two clusters of bursts for BATSE. These two groups resemble the short/hard and long/soft groups identified for *Swift*/BAT. Similarly to *Swift*/BAT, a KS test applied to the two BATSE groups reveals significant differences in their duration, hardness, peak energy and peak flux. BATSE has a harder energy range than *Swift*/BAT, and thus the BATSE population contains more short/hard bursts. Therefore for BATSE, the short duration Group 1 contains a larger proportion of bursts compared to *Swift*/BAT.

For *Fermi*/GBM, the projection in Figure 5c indicates two groups primarily consisting of short/hard and long/soft bursts, but their clustering is not dense enough to allow a clean separation between them. MCLUST identifies 5 clusters. This may indicate that the application of a Gaussian model does not adequately represent the underlying complex distributions [17].

5. Consistency Checks

The analysis of the first second of prompt emission (T_1) identifies two groups of bursts within the BATSE, *Swift*/BAT and *Fermi*/GBM samples. We focus this discussion on the more clear-cut results obtained with *Swift*/BAT.

5.1. T_{100} vs T_1 Analysis

For *Swift*/BAT, two groups are identified using both the T_{100} and T_1 intervals. Table 2 provides the classification results obtained with each interval. The sample sizes of the 2 groups are shown in Table 3, separated into long ($T_{90} > 2$ s) and short ($T_{90} < 2$ s) duration bursts.

Table 3. Sample sizes of short duration ($T_{90} < 2$ s) and long duration ($T_{90} > 2$ s) bursts in the *Swift*/BAT sample, and Groups 1 and 2, based on the analysis of the T_1 and the T_{100} intervals.

Sample	Number of bursts			
	$T_{90} < 2$ s		$T_{90} > 2$ s	
	T_1	T_{100}	T_1	T_{100}
Swift/BAT sample	107	107	1144	1147
Group 1	73	91	32	14
Group 2	34	16	1112	1133

95% (1185 of the 1251 bursts) of the classifications of *Swift*/BAT bursts determined using the T_1 interval at 4 ms resolution are consistent with those derived using the T_{100} intervals at 64 ms resolution. There are 21 short duration bursts which are classified as Group 2 bursts when the T_1 interval is considered, but move to Group 1 when the T_{100} interval is used for the analysis. There are 28 long duration bursts which move from Group 1 in the T_1 analysis to Group 2 when the T_{100} interval is considered. These include 5 bursts in the list of *Swift*/BAT bursts with extended emission episodes compiled by Gibson *et al.* [100]. The long duration supernova-accompanied burst GRB 101219B moves to Group 2 in the T_{100} analysis, correctly placing it amongst the other bursts with associated supernovae. The inclusion of the full light curve data in these cases is important for correct classification. The classification of bursts with associated supernovae is discussed further in Section 6. Some of the movement between groups may reflect the different temporal resolutions used for the T_1 (4 ms) and T_{100} (64 ms) analyses. The minimum variability timescale in short GRBs of order 10 ms, would not necessarily be captured by the T_{100} analysis. There may also be cases where there is pre-trigger emission that is not captured in the current approach which starts at the trigger time.

5.2. Inter-comparison of Swift/BAT and Fermi/GBM Results

In all 3 GRB samples, clear evidence of a separation into two groups by the end of the first second was observed. The clean separation of bursts in the *Swift*/BAT sample indicates that the T_1 interval could potentially be used to classify GRBs independently of their T_{90} duration. The less clear-cut cluster separation found in the BATSE and *Fermi*/GBM samples most likely arise from instrumental differences (e.g. energy ranges, triggering methods and sensitivities). Of the 3 instruments, *Swift*/BAT has the largest effective area, and detects more spectrally softer long duration GRBs [101], and fewer short GRBs, than BATSE or *Fermi*/GBM [80,102].

There are 293 bursts analysed which were detected by both *Fermi*/GBM and *Swift*/BAT. There is excellent (274/293) agreement between the 2 instruments in the cluster membership of these GRBs using the T_1 interval at 4 ms resolution. Differences in classification can be attributed primarily to the lack of clear separation between groups in the *Fermi*/GBM sample which makes cluster identification less definitive than for *Swift*/BAT. In 6 of the 19 cases where cluster membership is found to disagree between the two detectors, there are significantly different (>50%) T_{90} durations recorded by the instruments.

5.3. Time Intervals

The analysis was repeated for different intervals within the bursts to investigate the intervals in which classes may be identified in the *Swift*/BAT sample.

First, the feature extraction analysis with 4 ms resolution light curves was performed for the interval of T_0-1 s to T_0+1 s (Figure 8a). The addition of pre-trigger data is shown to produce almost identical results to those obtained by starting at T_0. However, the analysis requires additional Principal Components to explain the variance, indicating that including 1 second of data before the trigger is adding more noise than information. Secondly, when the selected interval is between $T_0+1.004$ s to $T_0+2.008$ s, the separation disappears, as shown in Figure 8b, indicating that the early prompt emission in the first second post-trigger is the key interval for separating the two classes.

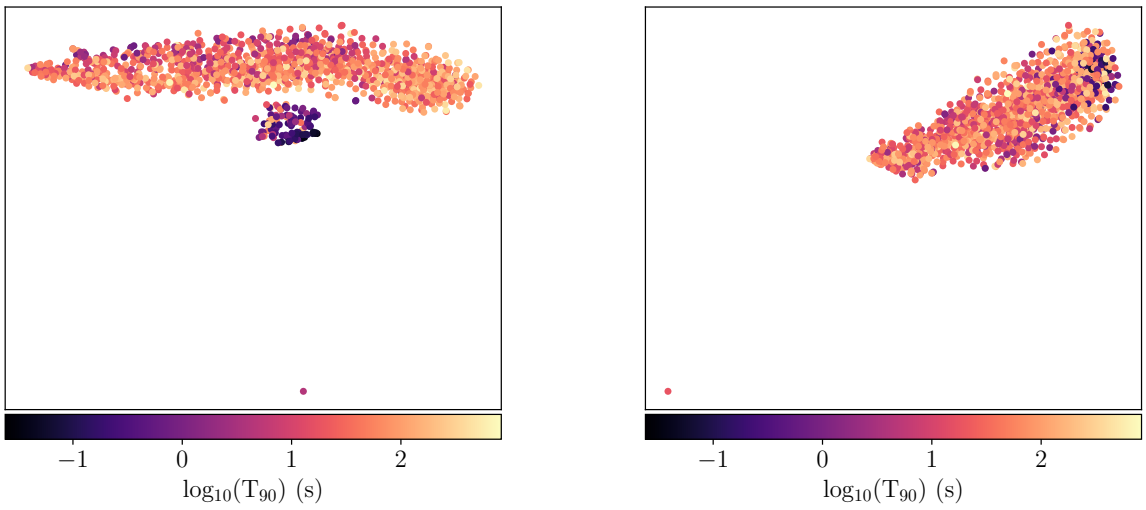

(a) **(b)**

Figure 8. 2D t-SNE representation of the wavelet feature extraction applied to *Swift*/BAT light curves covering time intervals (a) T_0-1 s to T_0+1 s and (b) T_0+1 s to T_0+2 s. The plots are coloured by burst duration T_{90}.

5.4. Light Curve Classifications

In Salmon *et al.* [17], Gaussian Mixture Model-based clustering of the hardness-T_{90} plane identified two classes of bursts in the *Swift*/BAT and *Fermi*/GBM samples. The results suggest that the intermediate duration class may be an artefact of the application of unsuitable models, also suggested by Tarnopolski [25], Koen and Bere [103], Tarnopolski [104,105]. The results of the model-independent analysis of light curves presented in this paper and by Jespersen *et al.* [33] lend further support to this conclusion.

Jespersen *et al.* [33] found two distinct groups of bursts in their t-SNE map obtained from Fourier decomposition of full *Swift*/BAT light curves. The composition of the 'type-S' and 'type-L' groups from Jespersen *et al.* [33] are compared to the clusters found in this work. For the T_{100} interval there is agreement in classification for 96% of bursts, after removing bursts for which no light curve files are available. Although the same burst intervals are considered, Jespersen *et al.* [33] input flux-normalised light curves into a Fourier-based analysis, potentially leading to small differences in the resulting burst

memberships compared to the wavelet-based analysis presented here. The light curves in this study were not flux normalised as the resulting t-SNE maps did not separate out the groups.

More than 96% of the bursts classified using wavelets and the T_1 interval are found to match the membership assigned by Jespersen *et al.* [33] based on Fourier decomposition in the T_{100} interval. Eight of the 20 bursts found to be within Group 1 in this study, that are classified as type-L by Jespersen *et al.* [33], have extended emission episodes which are not captured within the first second.

5.5. Collapsar 'Contamination'

The fraction of *Swift*/BAT bursts within Groups 1 and 2 can be compared to the expected distributions specific to the *Swift*/BAT detector.

Bromberg *et al.* [32] quantified the contamination of short GRB samples by collapsar bursts by fitting the duration distribution of *Swift* bursts with a function representing the merger and collapsar duration distributions. The model is based on the plateau in the duration distribution for durations less than the jet breakout time, which is predicted by the collapsar model [106]. According to this model ∼40% of *Swift*/BAT bursts with durations < 2 s are collapsar bursts. *Swift*/BAT is more sensitive to soft GRBs, meaning that low fluence long GRBs contaminate the short GRB population to a greater extent than for BATSE (∼10%) and *Fermi*/GBM (∼15%).

There are 27 bursts for which Bromberg *et al.* [32] assigns a probability of being a non-Collapsar of $> 90\%$. The majority (23) of these are classified as Group 1 in this analysis, indicating that Group 1 consists primarily of bursts arising from mergers. The collapsar (Group 2) contamination of *Swift*/BAT bursts with durations <2 s from our analysis of the first 1 s of prompt emission is 31.8%, or 34/107 bursts (Table 3), consistent within 1σ with the predictions in Bromberg *et al.* [32]. The collapsar contamination of short duration bursts for the T_{100} analysis is significantly lower at ∼15%. These results suggest that classification based on the T_1 interval may be useful for identifying collapsar 'imposters' in short GRB samples.

6. Notable GRBs

We discuss cluster membership for some notable GRBs. As a default, the discussion relates to results obtained with the T_1 interval at 4 ms resolution unless otherwise indicated. We identify cluster membership for GRBs in any of the 3 samples analysed which have associated kilonovae or supernovae. We note that cluster membership for the BATSE and *Fermi* samples is not as clear-cut as for the *Swift* sample, and the cut in t-SNE space is made by eye.

6.1. GRBs with Associated Supernovae

As discussed in Section 5.5, Group 2 is associated with collapsar bursts. Thus, it is expected that GRBs with associated supernovae will lie within Group 2. The list of 31 *Swift* and 10 *Fermi* Supernova (SN)-GRBs provided in Cano *et al.* [107] is extended to include additional SN-GRB events GRB 161219B/SN 2016jca [108], GRB 171205A/SN 2017htp [109], GRB 180728A/SN 2018fip [110,111], GRB 190114C/SN 2019jrj and GRB 190829A/AT2019oyw [112] and the peculiar short GRB 200826A [113–115]. Figure 9 indicates the location of these bursts within the t-SNE plot. The 25 SN-GRBs for which light curve files are available lie in Group 2 of *Swift*/BAT and *Fermi*/GBM as expected, with the exception of GRB 101219B which is an outlier to the *Swift*/BAT Group 1 but lies within Group 2 of *Fermi*/GBM bursts. The analysis using the T_{100} interval correctly places GRB 101219B in Group 2 for *Swift*/BAT. The shortest collapsar burst detected so far, GRB 200826A, lies within Group 2 of the *Fermi*/GBM sample despite its observed duration of $T_{90} \approx 0.96$ s [115].

The remaining bursts are identified in Group 2, with their classifications unchanged by the interval used in analysis, with the exception of GRB 050824 which migrates to Group 1 when the T_{100} interval is used for analysis.

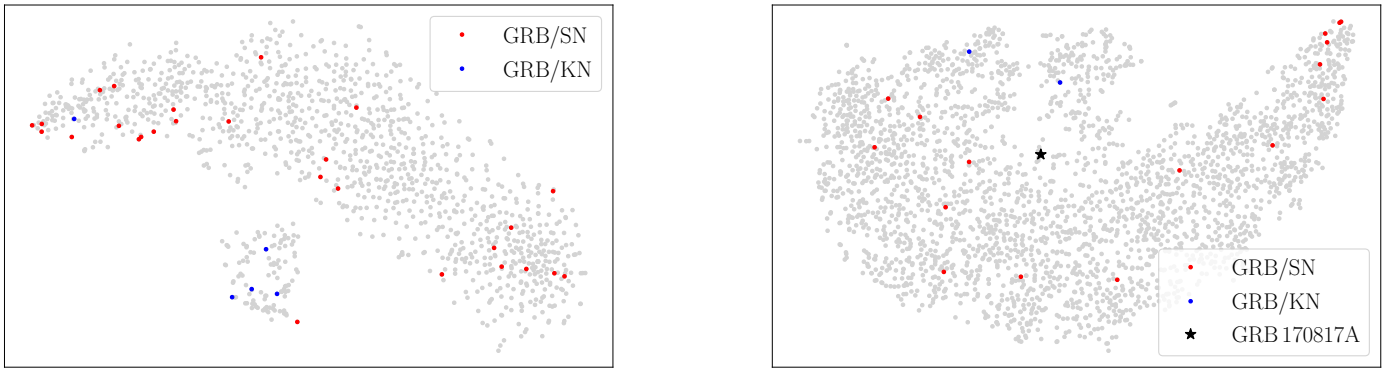

(a) **(b)**

Figure 9. Locations of GRBs with associated Supernovae (GRB/SN) and possible Kilonovae (GRB/KN) within the t-SNE projections of the T_1 interval for (a) *Swift*/BAT and (b) *Fermi*/GBM. The location of the only confirmed kilonova, associated with GRB 170817A, is indicated with a black star.

6.2. GRBs with Possible Kilonovae

The only confirmed kilonova is associated with GRB 170817A which is in the *Fermi*/GBM sample (Figure 9b) and does not clearly belong to either group. However, GRB 170817A was not a standard 'short' GRB, and would probably have been unremarked upon if not for the associated gravitational wave source [13,14]. Near-infrared excesses, similar to kilonova signatures, have been found in the afterglows of a handful of nearby short GRBs. Following the detection in GRB 130603B [116,117], reanalysis of GRB 060614 [118,119], GRB 080503 [120] and GRB 050709 [121] revealed similar near-IR components. Since then, GRB 150101B [122], GRB 160821B [123–126] and GRB 200522A [127] have all been suggested as kilonova candidates.

Figure 9 shows that all of the kilonova candidate bursts lie within Group 1 of *Swift* and *Fermi* GRBs, except for GRB 050709 for which no light curve file is available, and GRB 060614, which is in Group 2. GRB 060614 is an anomalous GRB with a short pulse followed by a longer period of soft flaring emission. Some properties of this burst are typical of the long GRB population [128], but the lack of a supernova detection for this close burst (z=0.125 Price *et al.* 129, Fugazza *et al.* 130) and possible near-infrared excess led to the suggestions that this burst originates from a merger [22], or is within its own subclass [131–135]. Our results agree with the classification by Jespersen *et al.* [33], who place this burst in the longer duration, collapsar, group. When the T_{100} light curve interval is considered, the classifications remain unchanged for the kilonova candidates, with the exception of GRB 080503 which moves to Group 2. This is an example of a GRB with a short initial spike and extended emission, that may be the result of a merger rather than a collapsar [120]. The T_1 interval appears to return the more appropriate classification in this case.

7. Discussion

Studies of GRB pulses at early times have revealed that the dominant radiation process is usually photospheric emission [136–141]. These thermal pulses exhibit significant spectral evolution, with bursts usually evolving to be dominated by synchrotron emission at later times [137,139,142]. If this is the case, the first second of all GRBs should be dominated by thermal pulses and therefore the radiation process itself is unlikely to be the driver of the observed differences in light curves appearing at early times.

The feature extraction algorithm may be identifying differences in the spectral evolution and pulse shapes of the two burst groups. The spectral lags of long and short bursts are different, with many short bursts exhibiting zero lag [18,63]. The minimum variability timescales for short and long bursts have also been found to be different [44–46]. For example Golkhou *et al.* [46] found median minimum variability timescales of 10 ms and 45 ms for short and long bursts, respectively. Hakkila and Preece [64] found that pulses in

short GRBs are shorter and harder than those in long GRBs, and exhibit more rapid spectral evolution. Coupled with the observation that shorter pulses have higher peak flux and $\sim 90\%$ of short GRBs consist of a single pulse, compared to 25–40% for long GRBs, pulse properties are likely to be a distinguishing feature in the first pulses and first seconds of a burst. Short GRBs have shorter pulse durations and their triple peaked substructure shows more intense precursor and decay peaks (on either side of the central peak) than long GRBs Hakkila *et al.* [56].

The magnitude of the PCA components in the different *Swift*/BAT energy bands indicate that Bands 2 and 3 contain the most variance, and therefore are the most important for the 4 ms light curves. Figure 10 shows the results of the feature extraction algorithm applied only to Band 3 data, showing that some segregation of the bursts into two groups is evident using light curves in one energy band. Thus, energy-dependent pulse characteristics are not the sole driver of the classification.

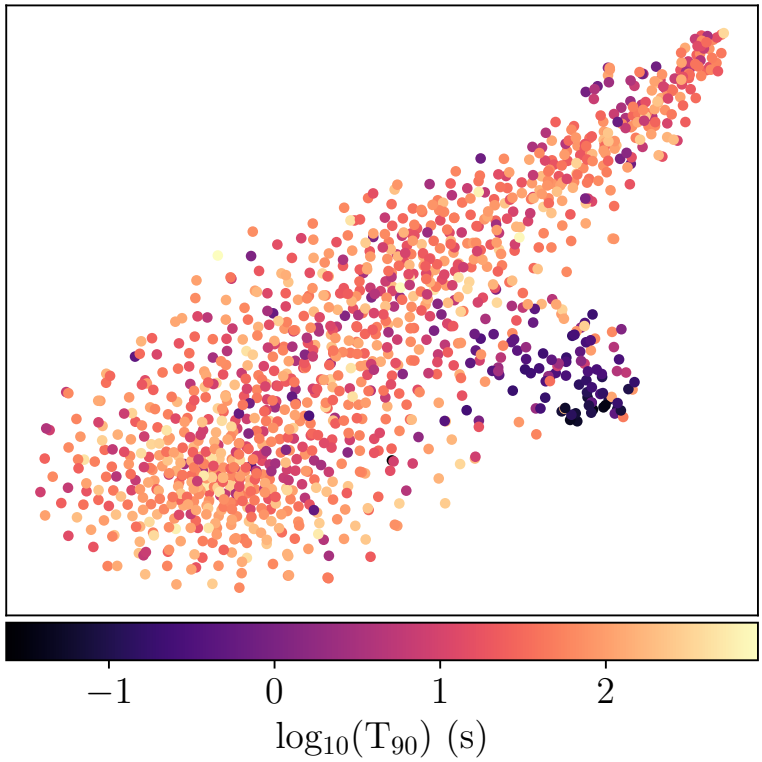

Figure 10. 2D t-SNE representation of the wavelet coefficients and PCA features extracted from the light curves measured in Band 3 for *Swift*/BAT (50–100 keV). The plot is coloured by burst duration T_{90}.

7.1. Cumulative Counts

Figure 6 shows that for the *Swift*/BAT sample, Group 1 and Group 2 GRBs identified within the T_1 interval consist mostly of bursts from the classical short duration ($T_{90} < 2$ s) and long duration ($T_{90} > 2$ s) samples, respectively. However, there are some 'strays', as shown in Table 3 and discussed in Section 5.

The counts measured in Band 3 (50–100 keV) of the first second of *Swift*/BAT 4 ms light curves are summed and normalised by the number of light curves, to obtain an average cumulative counts measure for bursts in each group in Table 3 (Figure 11). The cumulative counts of Group 1 and Group 2 bursts track those of short and long GRBs respectively during the first second.

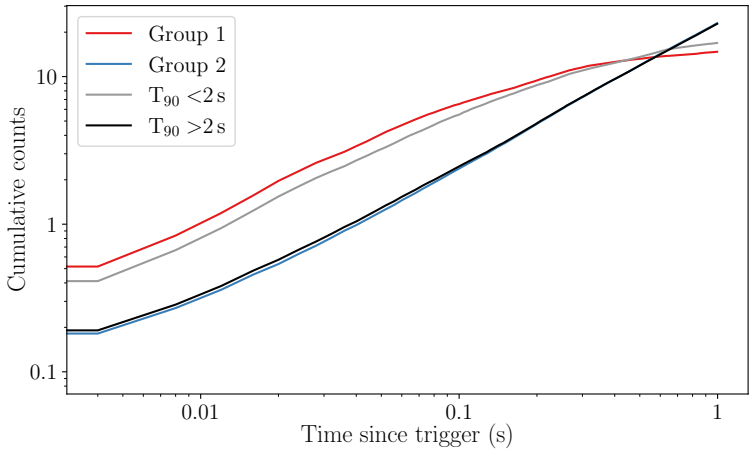

Figure 11. Normalised cumulative counts of Band 3 (50–100 keV) *Swift*/BAT 4 ms light curves. Short ($T_{90} < 2$ s) and long ($T_{90} > 2$ s) duration bursts, and those within the Groups 1 and 2 identified from the first 1 s of prompt emission, are shown.

The results of this analysis suggest that the behaviour of GRB pulses in the first second carries essential information needed to classify GRBs in the vast majority of cases, independent of their duration. The characteristics of the 'long' Group 1 and 'short' Group 2 bursts suggests that they have not been misclassified, but rather that they are duration outliers to their identified class. Group 1 and Group 2 bursts evolve in a similar way to the traditional short and long classes, respectively.

Previous studies have interpreted cumulative GRB light curves slope as a measure of the cumulative power output of the central engine [143]. Combined with the association of Group 1 and 2 bursts with kilonovae and supernovae respectively (Section 6), the cumulative counts behaviour in the first second suggests that Group 1 and 2 represent distinct progenitors, namely the merger and collapsar populations.

8. Conclusions

Wavelet decomposition combined with PCA and t-SNE provides an effective method for extracting the similarities between gamma-ray light curves from BATSE, *Swift*/BAT and *Fermi*/GBM. Features extracted from the T_{100} interval of light curves in four energy bands at 64 ms resolution reveal a separation between two groups of bursts. These groups are labelled Group 1 and Group 2. Two groups are also identified through feature extraction from high resolution (4 ms) light curves within the first seconds of prompt emission. The shortest timescale at which this separation is clear is one second (T_1 interval).

The separation between groups is clearest for *Swift*/BAT and is less distinct for the BATSE and *Fermi*/GBM samples of bursts, perhaps due to instrumental effects. Despite the different timescales and resolutions studied, there is $>$ 95% agreement between the groups identified within the T_{100} and T_1 interval for *Swift*/BAT. The T_{100} interval is shown to produce different and more classical classifications for some bursts, especially those with long emission episodes. There is also >95% agreement between the results of the T_1 analysis with the results of the Fourier-based feature extraction of *Swift*/BAT light curves by Jespersen *et al.* [33]. The separation between *Swift*/BAT groups is clearest when all four energy bands are considered. However energy-dependent characteristics are not the sole effect which drives the classification, as some separation can be seen when only one energy band is considered. Pulse shape and evolution may be important, and the accumulation of counts within the first second is found to be distinct between the groups.

Group 1 consists mostly of short duration, spectrally hard bursts. Group 2 consists of mostly spectrally soft, long duration bursts. When segmented at T_{90}=2 s, the traditional dividing line between long and short GRBs, we find that 99% (97%) of *Swift*/BAT Group

2 bursts have durations >2 s when the T_{100} (T_1) interval is used. 32% of the 107 GRBs with T_{90} <2 s are identified as Group 2 bursts when the T_1 interval is used, consistent (within 1σ) with a model in which the duration distribution of *Swift* bursts is fit with a function representing the merger and collapsar distributions, possibly reflecting the amount of collapsar 'contamination' in the short GRB sample. The observed contamination fraction is significantly lower (16%) when the T_{100} interval is used. Thus, the groups can be associated with distinct progenitors, namely mergers and collapsars. GRBs with associated supernovae are within Group 2, while GRBs with suspected kilonovae lie in Group 1.

Previous studies found that the pulse and spectral properties of the early seconds of long GRBs are similar to those of short GRBs. In this analysis, no significant differences in pulse or spectral properties can be identified to account for Group 1 and Group 2 GRBs being distinguishable in the T_1 interval. Differences in minimum variability timescale, identifiable only when the 4 ms resolution data are used, may account for some of the observed behaviour. However, the 2 groups in subsequent 1 s intervals should also be evident, which is not the case. The observed different slopes in the first second between the two groups in the combined cumulative counts may point towards differences in the central engine.

The results presented indicate that the nature of a burst may be inferred from the earliest prompt emission, without considering the full burst duration. Prompt classification will be helpful in the era of 'big data' in time-domain astronomy. Gravitational wave detectors will detect mergers at increased rates in the near and longer term [144]. State-of-the-art optical surveys such as the Vera Rubin Observatory will deliver an increased number of transient targets in the crowded optical sky [145]. While many optical transients are false positives, the rare gamma-ray transients can pinpoint the unambiguous target of interest. Early detection and classification of these gamma-ray transients will help to prioritise counterpart follow-up for optical telescopes and spectroscopic observations. Classification schemes and triggering algorithms could incorporate a wavelet-based analysis such as that presented here to prioritise targets for such follow-up observations.

Supplementary Materials: The following are available online at https://www.mdpi.com/article/10.3390/1010000/s1. The electronic version of this article showcases Figure 4 as three mp4 animations of the t-SNE plots for BATSE, *Swift* and *Fermi*. We provide the full version of Table 2 which includes the classification of *Swift*/BAT GRBs using the first second of prompt emission.

Author Contributions: Conceptualization, L.S., L.H. and A.M.C.; methodology, L.S., L.H. and A.M.C.; software, L.S.; validation, L.S., L.H., and A.M.C.; formal analysis, L.S.; investigation, L.S.; resources, L.S., L.H., and A.M.C.; data curation, L.S.; writing—original draft preparation, L.S.; writing—review and editing, L.H. and A.M.C.; visualization, L.S.; supervision, L.H. and A.M.C. ; project administration, L.H. and A.M.C. ; funding acquisition, L.H. and A.M.C. All authors have read and agreed to the published version of the manuscript.

Funding: LS acknowledges the Irish Research Council Postgraduate Scholarship No GOIPG/2017/1525. LH acknowledges support from Science Foundation Ireland (Grant number 19/FFP/6777) and the EU H2020 (Grant agreement 871158).

Institutional Review Board Statement: Not applicable.

Informed Consent Statement: Not applicable.

Data Availability Statement: The BATSE Public Data Archive (https://heasarc.gsfc.nasa.gov/FTP/compton/data/batse/trigger/, accessed on 17/02/21) hosts the 64 ms light curves in ascii files, and the TTE data which is used to generate the 4 ms BATSE light curves. The *Swift*/BAT light curves analysed in this paper are available as ascii files from the *Swift*/BAT Gamma-Ray Burst Catalogue[1]. The *Fermi*-GBM Data Tools [81] are used to access *Fermi*/GBM TTE files.

Acknowledgments: This research made use of the following Python packages : NumPy [146], Matplotlib [147], pandas [148,149], scikit-learn [150], GPFlow [83] and PyWavelets [89].

[1] https://swift.gsfc.nasa.gov/results/batgrbcat/

Conflicts of Interest: The authors declare no conflict of interest.The funders had no role in the design of the study; in the collection, analyses, or interpretation of data; in the writing of the manuscript, or in the decision to publish the results.

References

1. Kouveliotou, C.; Meegan, C.A.; Fishman, G.J.; Bhat, N.P.; Briggs, M.S.; Koshut, T.M.; Paciesas, W.S.; Pendleton, G.N. Identification of Two Classes of Gamma-Ray Bursts. *ApJ* **1993**, *413*, L101. doi:10.1086/186969.
2. Perley, D.A.; Niino, Y.; Tanvir, N.R.; Vergani, S.D.; Fynbo, J.P.U. Long-Duration Gamma-Ray Burst Host Galaxies in Emission and Absorption. *Space Sci. Rev.* **2016**, *202*, 111–142, [arXiv:astro-ph.HE/1602.00770]. doi:10.1007/s11214-016-0237-4.
3. Galama, T.J.; Vreeswijk, P.M.; van Paradijs, J.; Kouveliotou, C.; Augusteijn, T.; Böhnhardt, H.; Brewer, J.P.; Doublier, V.; Gonzalez, J.F.; Leibundgut, B.; et al. An unusual supernova in the error box of the γ-ray burst of 25 April 1998. *Nature* **1998**, *395*, 670–672, [arXiv:astro-ph/astro-ph/9806175]. doi:10.1038/27150.
4. Hjorth, J.; Sollerman, J.; Møller, P.; Fynbo, J.P.U.; Woosley, S.E.; Kouveliotou, C.; Tanvir, N.R.; Greiner, J.; Andersen, M.I.; Castro-Tirado, A.J.; et al. A very energetic supernova associated with the γ-ray burst of 29 March 2003. *Nature* **2003**, *423*, 847–850, [arXiv:astro-ph/astro-ph/0306347]. doi:10.1038/nature01750.
5. Stanek, K.Z.; Matheson, T.; Garnavich, P.M.; Martini, P.; Berlind, P.; Caldwell, N.; Challis, P.; Brown, W.R.; Schild, R.; Krisciunas, K.; et al. Spectroscopic Discovery of the Supernova 2003dh Associated with GRB 030329. *ApJ* **2003**, *591*, L17–L20, [arXiv:astro-ph/astro-ph/0304173]. doi:10.1086/376976.
6. Woosley, S.E.; Bloom, J.S. The Supernova Gamma-Ray Burst Connection. *ARA&A* **2006**, *44*, 507–556, [arXiv:astro-ph/astro-ph/0609142]. doi:10.1146/annurev.astro.43.072103.150558.
7. MacFadyen, A.I.; Woosley, S.E. Collapsars: Gamma-Ray Bursts and Explosions in "Failed Supernovae". *ApJ* **1999**, *524*, 262–289, [arXiv:astro-ph/astro-ph/9810274]. doi:10.1086/307790.
8. Eichler, D.; Livio, M.; Piran, T.; Schramm, D.N. Nucleosynthesis, neutrino bursts and γ-rays from coalescing neutron stars. *Nature* **1989**, *340*, 126–128. doi:10.1038/340126a0.
9. Narayan, R.; Paczynski, B.; Piran, T. Gamma-Ray Bursts as the Death Throes of Massive Binary Stars. *ApJ* **1992**, *395*, L83, [arXiv:astro-ph/astro-ph/9204001]. doi:10.1086/186493.
10. Berger, E. Short-Duration Gamma-Ray Bursts. *ARA&A* **2014**, *52*, 43–105, [arXiv:astro-ph.HE/1311.2603]. doi:10.1146/annurev-astro-081913-035926.
11. Berger, E. A Short Gamma-ray Burst "No-host" Problem? Investigating Large Progenitor Offsets for Short GRBs with Optical Afterglows. *ApJ* **2010**, *722*, 1946–1961, [arXiv:astro-ph.HE/1007.0003]. doi:10.1088/0004-637X/722/2/1946.
12. Tunnicliffe, R.L.; Levan, A.J.; Tanvir, N.R.; Rowlinson, A.; Perley, D.A.; Bloom, J.S.; Cenko, S.B.; O'Brien, P.T.; Cobb, B.E.; Wiersema, K.; et al. On the nature of the 'hostless' short GRBs. *MNRAS* **2014**, *437*, 1495–1510, [arXiv:astro-ph.HE/1402.0766]. doi:10.1093/mnras/stt1975.
13. Goldstein, A.; Veres, P.; Burns, E.; Briggs, M.S.; Hamburg, R.; Kocevski, D.; Wilson-Hodge, C.A.; Preece, R.D.; Poolakkil, S.; Roberts, O.J.; et al. An Ordinary Short Gamma-Ray Burst with Extraordinary Implications: Fermi-GBM Detection of GRB 170817A. *ApJ* **2017**, *848*, L14, [arXiv:astro-ph.HE/1710.05446]. doi:10.3847/2041-8213/aa8f41.
14. Savchenko, V.; Ferrigno, C.; Kuulkers, E.; Bazzano, A.; Bozzo, E.; Brandt, S.; Chenevez, J.; Courvoisier, T.L.; Diehl, R.; Domingo, A.; et al. INTEGRAL detection of the first prompt gamma-ray signal coincident with the gravitational-wave event GW170817. *ApJ* **2017**, *848*, L15, [arXiv:astro-ph.HE/1710.05449]. doi:10.3847/2041-8213/aa8f94.
15. Abbott, B.P.; Abbott, R.; Abbott, T.D.; Acernese, F.; Ackley, K.; Adams, C.; Adams, T.; Addesso, P.; Adhikari, R.X.; Adya, V.B.; et al. Multi-messenger Observations of a Binary Neutron Star Merger. *ApJ* **2017**, *848*, L12, [arXiv:astro-ph.HE/1710.05833]. doi:10.3847/2041-8213/aa91c9.
16. Horváth, I. A Third Class of Gamma-Ray Bursts? *ApJ* **1998**, *508*, 757–759, [arXiv:astro-ph/astro-ph/9803077]. doi:10.1086/306416.
17. Salmon, L.; Hanlon, L.; Martin-Carrillo, A. Two Dimensional Clustering of Swift/BAT and Fermi/GBM Gamma-ray Bursts. *Galaxies* **2022**, *10*. doi:10.3390/galaxies10040077.
18. Norris, J.P.; Bonnell, J.T. Short Gamma-Ray Bursts with Extended Emission. *ApJ* **2006**, *643*, 266–275, [arXiv:astro-ph/astro-ph/0601190]. doi:10.1086/502796.
19. Barkov, M.V.; Pozanenko, A.S. Model of the extended emission of short gamma-ray bursts. *MNRAS* **2011**, *417*, 2161–2165, [arXiv:astro-ph.HE/1103.4246]. doi:10.1111/j.1365-2966.2011.19398.x.
20. Norris, J.P.; Gehrels, N.; Scargle, J.D. Threshold for Extended Emission in Short Gamma-Ray Bursts. American Astronomical Society Meeting Abstracts #217, 2011, Vol. 217, *American Astronomical Society Meeting Abstracts*, p. 108.03.
21. D'Avanzo, P. Short gamma-ray bursts: A review. *Journal of High Energy Astrophysics* **2015**, *7*, 73–80. doi:10.1016/j.jheap.2015.07.002.
22. Zhang, B.; Zhang, B.B.; Liang, E.W.; Gehrels, N.; Burrows, D.N.; Mészáros, P. Making a Short Gamma-Ray Burst from a Long One: Implications for the Nature of GRB 060614. *ApJ* **2007**, *655*, L25–L28, [arXiv:astro-ph/astro-ph/0612238]. doi:10.1086/511781.
23. Zhang, B.; Zhang, B.B.; Virgili, F.J.; Liang, E.W.; Kann, D.A.; Wu, X.F.; Proga, D.; Lv, H.J.; Toma, K.; Mészáros, P.; et al. Discerning the Physical Origins of Cosmological Gamma-ray Bursts Based on Multiple Observational Criteria: The Cases of z = 6.7 GRB 080913, z = 8.2 GRB 090423, and Some Short/Hard GRBs. *ApJ* **2009**, *703*, 1696–1724, [arXiv:astro-ph.HE/0902.2419]. doi:10.1088/0004-637X/703/2/1696.

24. Li, Y.; Zhang, B.; Yuan, Q. A Comparative Study of Long and Short GRBs. II. A Multiwavelength Method to Distinguish Type II (Massive Star) and Type I (Compact Star) GRBs. *ApJ* **2020**, *897*, 154, [arXiv:astro-ph.HE/2005.13663]. doi:10.3847/1538-4357/ab96b8.
25. Tarnopolski, M. Distinguishing short and long Fermi gamma-ray bursts. *MNRAS* **2015**, *454*, 1132–1139, [arXiv:astro-ph.HE/1507.04886]. doi:10.1093/mnras/stv2061.
26. Goldstein, A.; Preece, R.D.; Briggs, M.S. A New Discriminator for Gamma-ray Burst Classification: The E_{peak}-fluence Energy Ratio. *ApJ* **2010**, *721*, 1329–1332, [arXiv:astro-ph.HE/1009.2105]. doi:10.1088/0004-637X/721/2/1329.
27. Qin, Y.P.; Chen, Z.F. Statistical classification of gamma-ray bursts based on the Amati relation. *MNRAS* **2013**, *430*, 163–173, [arXiv:astro-ph.HE/1311.4713]. doi:10.1093/mnras/sts547.
28. Lü, H.J.; Liang, E.W.; Zhang, B.B.; Zhang, B. A New Classification Method for Gamma-ray Bursts. *ApJ* **2010**, *725*, 1965–1970, [arXiv:astro-ph.HE/1001.0598]. doi:10.1088/0004-637X/725/2/1965.
29. Lü, H.J.; Zhang, B.; Liang, E.W.; Zhang, B.B.; Sakamoto, T. The 'amplitude' parameter of gamma-ray bursts and its implications for GRB classification. *MNRAS* **2014**, *442*, 1922–1929, [arXiv:astro-ph.HE/1211.1117]. doi:10.1093/mnras/stu982.
30. Zhang, S.; Shao, L.; Zhang, B.B.; Zou, J.H.; Sun, H.Y.; Yao, Y.J.; Li, L.L. A Tight Three-parameter Correlation and Related Classification on Gamma-Ray Bursts. *arXiv e-prints* **2022**, p. arXiv:2201.10861, [arXiv:astro-ph.HE/2201.10861].
31. Hakkila, J.; Giblin, T.W.; Roiger, R.J.; Haglin, D.J.; Paciesas, W.S.; Meegan, C.A. How Sample Completeness Affects Gamma-Ray Burst Classification. *ApJ* **2003**, *582*, 320–329, [arXiv:astro-ph/astro-ph/0209073]. doi:10.1086/344568.
32. Bromberg, O.; Nakar, E.; Piran, T.; Sari, R. Short versus Long and Collapsars versus Non-collapsars: A Quantitative Classification of Gamma-Ray Bursts. *ApJ* **2013**, *764*, 179, [arXiv:astro-ph.HE/1210.0068]. doi:10.1088/0004-637X/764/2/179.
33. Jespersen, C.K.; Severin, J.B.; Steinhardt, C.L.; Vinther, J.; Fynbo, J.P.U.; Selsing, J.; Watson, D. An Unambiguous Separation of Gamma-Ray Bursts into Two Classes from Prompt Emission Alone. *ApJ* **2020**, *896*, L20, [arXiv:astro-ph.HE/2005.13554]. doi:10.3847/2041-8213/ab964d.
34. Mallat, S.G. A theory for multiresolution signal decomposition - The wavelet representation. *IEEE Transactions on Pattern Analysis and Machine Intelligence* **1989**, *11*, 674–693.
35. Meredith, D.C.; Ryan, J.M.; Young, C.A.; Lestrade, J.P. Wavelet Analysis of Gamma Ray Bursts. Gamma-Ray Bursts; Fishman, G.J., Ed., 1994, Vol. 307, *American Institute of Physics Conference Series*, p. 701. doi:10.1063/1.45915.
36. Young, C.A.; Meredith, D.C.; Ryan, J.M. A Compact Representation of Gamma-Ray Burst Time Series. *Ap&SS* **1995**, *231*, 119–122. doi:10.1007/BF00658599.
37. Bagoly, Z.; Balázs, L.G.; Horváth, I.; Mészáros, A. Wavelet Analysis of the BATSE 64ms GRB Lightcurves. Gamma-Ray Bursts in the Afterglow Era; Feroci, M.; Frontera, F.; Masetti, N.; Piro, L., Eds., 2004, Vol. 312, *Astronomical Society of the Pacific Conference Series*, p. 51.
38. Hurley, K.J.; McBreen, B.; Quilligan, F.; Delaney, M.; Hanlon, L. Wavelet analysis and lognormal distributions in GRBs. Gamma-Ray Bursts, 4th Hunstville Symposium; Meegan, C.A.; Preece, R.D.; Koshut, T.M., Eds., 1998, Vol. 428, *American Institute of Physics Conference Series*, pp. 191–195, [arXiv:astro-ph/astro-ph/9807219]. doi:10.1063/1.55319.
39. Quilligan, F.; Hurley, K.J.; McBreen, B.; Hanlon, L.; Duggan, P. Characteristic properties of peaks in GRBs. *A&AS* **1999**, *138*, 419–420. doi:10.1051/aas:1999291.
40. Quilligan, F.; McBreen, B.; Hanlon, L.; McBreen, S.; Hurley, K.J.; Watson, D. Temporal properties of gamma ray bursts as signatures of jets from the central engine. *A&A* **2002**, *385*, 377–398, [arXiv:astro-ph/astro-ph/0112515]. doi:10.1051/0004-6361:20020038.
41. Qin, Y.P.; Liang, E.W.; Xie, G.Z.; Su, C.Y. Statistical Properties of the Highest Pulses in Gamma-Ray Bursts. *Chinese J. Astron. Astrophys.* **2003**, *3*, 38–48, [arXiv:astro-ph/astro-ph/0209525]. doi:10.1088/1009-9271/3/1/38.
42. Walker, K.C.; Schaefer, B.E.; Fenimore, E.E. Gamma-Ray Bursts Have Millisecond Variability. *ApJ* **2000**, *537*, 264–269, [arXiv:astro-ph/astro-ph/9810271]. doi:10.1086/308995.
43. MacLachlan, G.A.; Shenoy, A.; Sonbas, E.; Dhuga, K.S.; Eskandarian, A.; Maximon, L.C.; Parke, W.C. The minimum variability time-scale and its relation to pulse profiles of Fermi GRBs. *MNRAS* **2012**, *425*, L32–L35, [arXiv:astro-ph.HE/1205.0055]. doi:10.1111/j.1745-3933.2012.01295.x.
44. MacLachlan, G.A.; Shenoy, A.; Sonbas, E.; Dhuga, K.S.; Cobb, B.E.; Ukwatta, T.N.; Morris, D.C.; Eskandarian, A.; Maximon, L.C.; Parke, W.C. Minimum variability time-scales of long and short GRBs. *MNRAS* **2013**, *432*, 857–865, [arXiv:astro-ph.HE/1201.4431]. doi:10.1093/mnras/stt241.
45. Golkhou, V.Z.; Butler, N.R. Uncovering the Intrinsic Variability of Gamma-Ray Bursts. *ApJ* **2014**, *787*, 90, [arXiv:astro-ph.HE/1403.4254]. doi:10.1088/0004-637X/787/1/90.
46. Golkhou, V.Z.; Butler, N.R.; Littlejohns, O.M. The Energy Dependence of GRB Minimum Variability Timescales. *ApJ* **2015**, *811*, 93, [arXiv:astro-ph.HE/1501.05948]. doi:10.1088/0004-637X/811/2/93.
47. Varughese, M.M.; von Sachs, R.; Stephanou, M.; Bassett, B.A. Non-parametric transient classification using adaptive wavelets. *MNRAS* **2015**, *453*, 2848–2861, [arXiv:astro-ph.IM/1504.00015]. doi:10.1093/mnras/stv1816.
48. Lochner, M.; McEwen, J.D.; Peiris, H.V.; Lahav, O.; Winter, M.K. Photometric Supernova Classification with Machine Learning. *ApJS* **2016**, *225*, 31, [arXiv:astro-ph.IM/1603.00882]. doi:10.3847/0067-0049/225/2/31.
49. Vargas dos Santos, M.; Quartin, M.; Reis, R.R.R. On the cosmological performance of photometrically classified supernovae with machine learning. *MNRAS* **2020**, *497*, 2974–2991, [arXiv:astro-ph.CO/1908.04210]. doi:10.1093/mnras/staa1968.

50. Norris, J.P.; Share, G.H.; Messina, D.C.; Dennis, B.R.; Desai, U.D.; Cline, T.L.; Matz, S.M.; Chupp, E.L. Spectral Evolution of Pulse Structures in Gamma-Ray Bursts. *ApJ* **1986**, *301*, 213. doi:10.1086/163889.
51. Golenetskii, S.V.; Mazets, E.P.; Aptekar, R.L.; Ilinskii, V.N. Correlation between luminosity and temperature in γ-ray burst sources. *Nature* **1983**, *306*, 451–453. doi:10.1038/306451a0.
52. Fenimore, E.E.; in 't Zand, J.J.M.; Norris, J.P.; Bonnell, J.T.; Nemiroff, R.J. Gamma-Ray Burst Peak Duration as a Function of Energy. *ApJ* **1995**, *448*, L101, [arXiv:astro-ph/astro-ph/9504075]. doi:10.1086/309603.
53. Nemiroff, R.J.; Norris, J.P.; Kouveliotou, C.; Fishman, G.J.; Meegan, C.A.; Paciesas, W.S. Gamma-Ray Bursts Are Time-asymmetric. *ApJ* **1994**, *423*, 432, [arXiv:astro-ph/astro-ph/9311050]. doi:10.1086/173819.
54. Norris, J.P.; Nemiroff, R.J.; Bonnell, J.T.; Scargle, J.D.; Kouveliotou, C.; Paciesas, W.S.; Meegan, C.A.; Fishman, G.J. Attributes of Pulses in Long Bright Gamma-Ray Bursts. *ApJ* **1996**, *459*, 393. doi:10.1086/176902.
55. Hakkila, J.; Preece, R.D. Unification of Pulses in Long and Short Gamma-Ray Bursts: Evidence from Pulse Properties and Their Correlations. *ApJ* **2011**, *740*, 104, [arXiv:astro-ph.HE/1103.5434]. doi:10.1088/0004-637X/740/2/104.
56. Hakkila, J.; Horváth, I.; Hofesmann, E.; Lesage, S. Properties of Short Gamma-ray Burst Pulses from a BATSE TTE GRB Pulse Catalog. *ApJ* **2018**, *855*, 101, [arXiv:astro-ph.HE/1710.08957]. doi:10.3847/1538-4357/aaac2b.
57. Cheng, L.X.; Ma, Y.Q.; Cheng, K.S.; Lu, T.; Zhou, Y.Y. The time delay of gamma-ray bursts in the soft energy band. *A&A* **1995**, *300*, 746.
58. Norris, J.P.; Marani, G.F.; Bonnell, J.T. Connection between Energy-dependent Lags and Peak Luminosity in Gamma-Ray Bursts. *ApJ* **2000**, *534*, 248–257, [arXiv:astro-ph/astro-ph/9903233]. doi:10.1086/308725.
59. Wu, B.; Fenimore, E. Spectral Lags of Gamma-Ray Bursts From Ginga and BATSE. *ApJ* **2000**, *535*, L29–L32, [arXiv:astro-ph/astro-ph/9908281]. doi:10.1086/312700.
60. Ukwatta, T.N.; Dhuga, K.S.; Stamatikos, M.; Dermer, C.D.; Sakamoto, T.; Sonbas, E.; Parke, W.C.; Maximon, L.C.; Linnemann, J.T.; Bhat, P.N.; et al. The lag-luminosity relation in the GRB source frame: an investigation with Swift BAT bursts. *MNRAS* **2012**, *419*, 614–623, [arXiv:astro-ph.HE/1109.0666]. doi:10.1111/j.1365-2966.2011.19723.x.
61. Ukwatta, T.N.; Stamatikos, M.; Dhuga, K.S.; Sakamoto, T.; Barthelmy, S.D.; Eskandarian, A.; Gehrels, N.; Maximon, L.C.; Norris, J.P.; Parke, W.C. Spectral Lags and the Lag-Luminosity Relation: An Investigation with Swift BAT Gamma-ray Bursts. *ApJ* **2010**, *711*, 1073–1086, [arXiv:astro-ph.HE/0908.2370]. doi:10.1088/0004-637X/711/2/1073.
62. Hakkila, J.; Giblin, T.W.; Norris, J.P.; Fragile, P.C.; Bonnell, J.T. Correlations between Lag, Luminosity, and Duration in Gamma-Ray Burst Pulses. *ApJ* **2008**, *677*, L81, [arXiv:astro-ph/0803.1655]. doi:10.1086/588094.
63. Bernardini, M.G.; Ghirlanda, G.; Campana, S.; Covino, S.; Salvaterra, R.; Atteia, J.L.; Burlon, D.; Calderone, G.; D'Avanzo, P.; D'Elia, V.; et al. Comparing the spectral lag of short and long gamma-ray bursts and its relation with the luminosity. *MNRAS* **2015**, *446*, 1129–1138, [arXiv:astro-ph.HE/1410.5216]. doi:10.1093/mnras/stu2153.
64. Hakkila, J.; Preece, R.D. Gamma-Ray Burst Pulse Shapes: Evidence for Embedded Shock Signatures? *ApJ* **2014**, *783*, 88, [arXiv:astro-ph.HE/1401.4047]. doi:10.1088/0004-637X/783/2/88.
65. Bhat, P.N.; Fishman, G.J.; Meegan, C.A.; Wilson, R.B.; Kouveliotou, C.; Paciesas, W.S.; Pendleton, G.N.; Schaefer, B.E. Spectral Evolution of a Subclass of Gamma-Ray Bursts Observed by BATSE. *ApJ* **1994**, *426*, 604. doi:10.1086/174097.
66. Band, D.L. Gamma-Ray Burst Spectral Evolution through Cross-Correlations of Discriminator Light Curves. *ApJ* **1997**, *486*, 928–937, [arXiv:astro-ph/astro-ph/9704206]. doi:10.1086/304566.
67. Ford, L.A.; Band, D.L.; Matteson, J.L.; Briggs, M.S.; Pendleton, G.N.; Preece, R.D.; Paciesas, W.S.; Teegarden, B.J.; Palmer, D.M.; Schaefer, B.E.; et al. BATSE Observations of Gamma-Ray Burst Spectra. II. Peak Energy Evolution in Bright, Long Bursts. *ApJ* **1995**, *439*, 307, [arXiv:astro-ph/astro-ph/9407090]. doi:10.1086/175174.
68. Borgonovo, L.; Ryde, F. On the Hardness-Intensity Correlation in Gamma-Ray Burst Pulses. *ApJ* **2001**, *548*, 770–786, [arXiv:astro-ph/astro-ph/0009164]. doi:10.1086/319008.
69. Peng, Z.Y.; Ma, L.; Lu, R.J.; Fang, L.M.; Bao, Y.Y.; Yin, Y. Spectral hardness evolution characteristics of tracking gamma-ray burst pulses. *New Astron.* **2009**, *14*, 311–320, [arXiv:astro-ph/0809.3620]. doi:10.1016/j.newast.2008.09.004.
70. Lu, R.J.; Hou, S.J.; Liang, E.W. The E $_p$-flux Correlation in the Rising and Decaying Phases of gamma-ray Burst Pulses: Evidence for Viewing Angle Effect? *ApJ* **2010**, *720*, 1146–1154, [arXiv:astro-ph.GA/1005.4242]. doi:10.1088/0004-637X/720/2/1146.
71. Hakkila, J.; Lien, A.; Sakamoto, T.; Morris, D.; Neff, J.E.; Giblin, T.W. Swift Observations of Gamma-Ray Burst Pulse Shapes: GRB Pulse Spectral Evolution Clarified. *ApJ* **2015**, *815*, 134, [arXiv:astro-ph.HE/1511.03695]. doi:10.1088/0004-637X/815/2/134.
72. Ghirlanda, G.; Nava, L.; Ghisellini, G. Spectral-luminosity relation within individual Fermi gamma rays bursts. *A&A* **2010**, *511*, A43, [arXiv:astro-ph.HE/0908.2807]. doi:10.1051/0004-6361/200913134.
73. Ghirlanda, G.; Ghisellini, G.; Nava, L.; Burlon, D. Spectral evolution of Fermi/GBM short gamma-ray bursts. *MNRAS* **2011**, *410*, L47–L51, [arXiv:astro-ph.HE/1008.4767]. doi:10.1111/j.1745-3933.2010.00977.x.
74. Lu, R.J.; Wei, J.J.; Liang, E.W.; Zhang, B.B.; Lü, H.J.; Lü, L.Z.; Lei, W.H.; Zhang, B. A Comprehensive Analysis of Fermi Gamma-Ray Burst Data. II. E $_p$ Evolution Patterns and Implications for the Observed Spectrum-Luminosity Relations. *ApJ* **2012**, *756*, 112, [arXiv:astro-ph.HE/1204.0714]. doi:10.1088/0004-637X/756/2/112.
75. Kocevski, D.; Petrosian, V. On the Lack of Time Dilation Signatures in Gamma-Ray Burst Light Curves. *ApJ* **2013**, *765*, 116. doi:10.1088/0004-637X/765/2/116.
76. Littlejohns, O.M.; Tanvir, N.R.; Willingale, R.; Evans, P.A.; O'Brien, P.T.; Levan, A.J. Are gamma-ray bursts the same at high redshift and low redshift? *MNRAS* **2013**, *436*, 3640–3655, [arXiv:astro-ph.HE/1309.7045]. doi:10.1093/mnras/stt1841.

77. Fishman, G.; et al. Gamma Ray Observatory Science Workshop. *Greenbelt (Ed.: WN Johnson, 1989)* **1989**, pp. 2–39.
78. Gehrels, N.; Chincarini, G.; Giommi, P.; Mason, K.O.; Nousek, J.A.; Wells, A.A.; White, N.E.; Barthelmy, S.D.; Burrows, D.N.; Cominsky, L.R.; et al. The Swift Gamma-Ray Burst Mission. *ApJ* **2004**, *611*, 1005–1020, [arXiv:astro-ph/astro-ph/0405233]. doi:10.1086/422091.
79. Meegan, C.; Lichti, G.; Bhat, P.N.; Bissaldi, E.; Briggs, M.S.; Connaughton, V.; Diehl, R.; Fishman, G.; Greiner, J.; Hoover, A.S.; et al. The Fermi Gamma-ray Burst Monitor. *ApJ* **2009**, *702*, 791–804, [arXiv:astro-ph.IM/0908.0450]. doi:10.1088/0004-637X/702/1/791.
80. Lien, A.; Sakamoto, T.; Barthelmy, S.D.; Baumgartner, W.H.; Cannizzo, J.K.; Chen, K.; Collins, N.R.; Cummings, J.R.; Gehrels, N.; Krimm, H.A.; et al. The Third Swift Burst Alert Telescope Gamma-Ray Burst Catalog. *ApJ* **2016**, *829*, 7, [arXiv:astro-ph.HE/1606.01956]. doi:10.3847/0004-637X/829/1/7.
81. Goldstein, A.; Cleveland, W.H.; Kocevski, D. Fermi GBM Data Tools: v1.04, 2020.
82. Sacks, J.; Welch, W.J.; Mitchell, T.J.; Wynn, H.P. Design and analysis of computer experiments. *Statistical science* **1989**, pp. 409–423.
83. De G. Matthews, A.G.; Van Der Wilk, M.; Nickson, T.; Fujii, K.; Boukouvalas, A.; León-Villagrá, P.; Ghahramani, Z.; Hensman, J. GPflow: A Gaussian process library using TensorFlow. *The Journal of Machine Learning Research* **2017**, *18*, 1299–1304.
84. Abadi, M.; Agarwal, A.; Barham, P.; Brevdo, E.; Chen, Z.; Citro, C.; Corrado, G.S.; Davis, A.; Dean, J.; Devin, M.; et al. TensorFlow: Large-Scale Machine Learning on Heterogeneous Systems, 2015. Software available from tensorflow.org.
85. Daubechies, I. *Ten lectures on wavelets*; SIAM, 1992.
86. Holschneider, M.; Kronland-Martinet, R.; Morlet, J.; Tchamitchian, P. A Real-Time Algorithm for Signal Analysis with the Help of the Wavelet Transform. Wavelets. Time-Frequency Methods and Phase Space; Combes, J.M.; Grossmann, A.; Tchamitchian, P., Eds., 1989, p. 286.
87. Addison, P.S. *The illustrated wavelet transform handbook: introductory theory and applications in science, engineering, medicine and finance*; CRC press, 2017.
88. Rhif, M.; Ben Abbes, A.; Farah, I.R.; Martínez, B.; Sang, Y. Wavelet transform application for/in non-stationary time-series analysis: a review. *Applied Sciences* **2019**, *9*, 1345.
89. Lee, G.; Gommers, R.; Waselewski, F.; Wohlfahrt, K.; O'Leary, A. PyWavelets: A Python package for wavelet analysis. *The Journal of Open Source Software* **2019**, *4*, 1237. doi:10.21105/joss.01237.
90. Daubechies, I. Orthonormal bases of compactly supported wavelets. *Communications on Pure and Applied Mathematics* **1988**, *41*, 909–996.
91. Pearson, K. LIII. On lines and planes of closest fit to systems of points in space. *The London, Edinburgh, and Dublin Philosophical Magazine and Journal of Science* **1901**, *2*, 559–572.
92. Hotelling, H. Analysis of a complex of statistical variables into principal components. *Journal of Educational Psychology* **1933**, *24*, 417.
93. Hinton, G.E.; Roweis, S.T. Stochastic neighbor embedding. *Advances in Neural Information Processing Systems* **2003**, p. 857–864.
94. Kullback, S.; Leibler, R.A. On Information and Sufficiency. *The Annals of Mathematical Statistics* **1951**, *22*, 79 – 86. doi:10.1214/aoms/1177729694.
95. Maaten, L.v.d.; Hinton, G. Visualizing data using t-SNE. *Journal of Machine Learning Research* **2008**, *9*, 2579–2605.
96. Fraley, C.; Raftery, A.E. MCLUST: Software for model-based cluster analysis. *Journal of classification* **1999**, *16*, 297–306.
97. Scrucca, L.; Fop, M.; Murphy, T.B.; Raftery, A.E. mclust 5: clustering, classification and density estimation using Gaussian finite mixture models. *The R Journal* **2016**, *8*, 289–317.
98. Schwarz, G.; et al. Estimating the dimension of a model. *The Annals of Statistics* **1978**, *6*, 461–464.
99. Baudry, J.P.; Raftery, A.E.; Celeux, G.; Lo, K.; Gottardo, R. Combining Mixture Components for Clustering. *Journal of Computational and Graphical Statistics* **2010**, *19*, 332–353, [https://doi.org/10.1198/jcgs.2010.08111]. doi:10.1198/jcgs.2010.08111.
100. Gibson, S.L.; Wynn, G.A.; Gompertz, B.P.; O'Brien, P.T. Fallback accretion on to a newborn magnetar: short GRBs with extended emission. *MNRAS* **2017**, *470*, 4925–4940, [arXiv:astro-ph.HE/1706.04802]. doi:10.1093/mnras/stx1531.
101. Racusin, J.L.; Oates, S.R.; Schady, P.; Burrows, D.N.; de Pasquale, M.; Donato, D.; Gehrels, N.; Koch, S.; McEnery, J.; Piran, T.; et al. Fermi and Swift Gamma-ray Burst Afterglow Population Studies. *ApJ* **2011**, *738*, 138, [arXiv:astro-ph.HE/1106.2469]. doi:10.1088/0004-637X/738/2/138.
102. Burgess, J.M.; Greiner, J.; Bégué, D.; Giannios, D.; Berlato, F.; Lipunov, V.M. Viewing Short Gamma-Ray Bursts From a Different Angle. *Frontiers in Astronomy and Space Sciences* **2020**, *7*, 40, [arXiv:astro-ph.HE/1710.05823]. doi:10.3389/fspas.2020.00040.
103. Koen, C.; Bere, A. On multiple classes of gamma-ray bursts, as deduced from autocorrelation functions or bivariate duration/hardness ratio distributions. *MNRAS* **2012**, *420*, 405–415. doi:10.1111/j.1365-2966.2011.20045.x.
104. Tarnopolski, M. Analysis of gamma-ray burst duration distribution using mixtures of skewed distributions. *Monthly Notices of the Royal Astronomical Society* **2016**, *458*, 2024–2031, [arXiv:astro-ph.HE/1506.07801]. doi:https://doi.org/10.1093/mnras/stw429.
105. Tarnopolski, M. Analysis of the Duration-Hardness Ratio Plane of Gamma-Ray Bursts Using Skewed Distributions. *ApJ* **2019**, *870*, 105, [arXiv:astro-ph.HE/1811.06745]. doi:10.3847/1538-4357/aaf1c5.
106. Bromberg, O.; Nakar, E.; Piran, T.; Sari, R. An Observational Imprint of the Collapsar Model of Long Gamma-Ray Bursts. *ApJ* **2012**, *749*, 110, [arXiv:astro-ph.HE/1111.2990]. doi:10.1088/0004-637X/749/2/110.
107. Cano, Z.; Wang, S.Q.; Dai, Z.G.; Wu, X.F. The Observer's Guide to the Gamma-Ray Burst Supernova Connection. *Advances in Astronomy* **2017**, *2017*, 8929054, [arXiv:astro-ph.HE/1604.03549]. doi:10.1155/2017/8929054.

108. Ashall, C.; Mazzali, P.A.; Pian, E.; Woosley, S.E.; Palazzi, E.; Prentice, S.J.; Kobayashi, S.; Holmbo, S.; Levan, A.; Perley, D.; et al. GRB 161219B/SN 2016jca: a powerful stellar collapse. *MNRAS* **2019**, *487*, 5824–5839, [arXiv:astro-ph.HE/1702.04339]. doi:10.1093/mnras/stz1588.
109. Melandri, A.; Malesani, D.B.; Izzo, L.; Japelj, J.; Vergani, S.D.; Schady, P.; Sagués Carracedo, A.; de Ugarte Postigo, A.; Anderson, J.P.; Barbarino, C.; et al. GRB 171010A/SN 2017htp: a GRB-SN at z = 0.33. *MNRAS* **2019**, *490*, 5366–5374, [arXiv:astro-ph.HE/1910.14160]. doi:10.1093/mnras/stz2900.
110. Izzo, L.; Rossi, A.; Malesani, D.; Heintz, K.; Selsing, J.; Schady, P.; Starling, R.; Sollerman, J.; Leloudas, G.; Cano, Z.; et al. GRB 180728A: discovery of the associated supernova. *GRB Coordinates Network* **2018**, *23142*, 1.
111. Selsing, J.; Izzo, L.; Rossi, A.; Malesani, D.; Heintz, K.; Schady, P.; Starling, R.; Sollerman, J.; Leloudas, G.; Cano, Z.; et al. GRB 180728A: classification of the associated SN 2018fip. *GRB Coordinates Network* **2018**, *23181*, 1.
112. Hu, Y.D.; Castro-Tirado, A.J.; Kumar, A.; Gupta, R.; Valeev, A.F.; Pandey, S.B.; Kann, D.A.; Castellón, A.; Agudo, I.; Aryan, A.; et al. 10.4 m GTC observations of the nearby VHE-detected GRB 190829A/SN 2019oyw. *A&A* **2021**, *646*, A50, [arXiv:astro-ph.HE/2009.04021]. doi:10.1051/0004-6361/202039349.
113. Ahumada, T.; Singer, L.P.; Anand, S.; Coughlin, M.W.; Kasliwal, M.M.; Ryan, G.; Andreoni, I.; Cenko, S.B.; Fremling, C.; Kumar, H.; et al. Discovery and confirmation of the shortest gamma ray burst from a collapsar. *arXiv e-prints* **2021**, p. arXiv:2105.05067, [arXiv:astro-ph.HE/2105.05067].
114. Rossi, A.; Rothberg, B.; Palazzi, E.; Kann, D.A.; D'Avanzo, P.; Klose, S.; Perego, A.; Pian, E.; Savaglio, S.; Stratta, G.; et al. The peculiar short-duration GRB 200826A and its supernova. *arXiv e-prints* **2021**, p. arXiv:2105.03829, [arXiv:astro-ph.HE/2105.03829].
115. Zhang, B.B.; Liu, Z.K.; Peng, Z.K.; Li, Y.; Lü, H.J.; Yang, J.; Yang, Y.S.; Yang, Y.H.; Meng, Y.Z.; Zou, J.H.; et al. A Peculiarly Short-duration Gamma-Ray Burst from Massive Star Core Collapse. *arXiv e-prints* **2021**, p. arXiv:2105.05021, [arXiv:astro-ph.HE/2105.05021].
116. Berger, E.; Fong, W.; Chornock, R. An r-process Kilonova Associated with the Short-hard GRB 130603B. *ApJ* **2013**, *774*, L23, [arXiv:astro-ph.HE/1306.3960]. doi:10.1088/2041-8205/774/2/L23.
117. Tanvir, N.R.; Levan, A.J.; Fruchter, A.S.; Hjorth, J.; Hounsell, R.A.; Wiersema, K.; Tunnicliffe, R.L. A 'kilonova' associated with the short-duration γ-ray burst GRB 130603B. *Nature* **2013**, *500*, 547–549, [arXiv:astro-ph.HE/1306.4971]. doi:10.1038/nature12505.
118. Jin, Z.P.; Fan, Y.Z.; Wei, D.M. An r- process macronova/kilonova in GRB 060614: evidence for the merger of a neutron star-black hole binary. EPJ Web of Conferences. EDP Sciences, 2016, Vol. 109, p. 08002, [arXiv:astro-ph.HE/1512.04192].
119. Yang, B.; Jin, Z.P.; Li, X.; Covino, S.; Zheng, X.Z.; Hotokezaka, K.; Fan, Y.Z.; Piran, T.; Wei, D.M. A possible macronova in the late afterglow of the long-short burst GRB 060614. *Nature Communications* **2015**, *6*, 7323, [arXiv:astro-ph.HE/1503.07761]. doi:10.1038/ncomms8323.
120. Perley, D.A.; Metzger, B.D.; Granot, J.; Butler, N.R.; Sakamoto, T.; Ramirez-Ruiz, E.; Levan, A.J.; Bloom, J.S.; Miller, A.A.; Bunker, A.; et al. GRB 080503: Implications of a Naked Short Gamma-Ray Burst Dominated by Extended Emission. *ApJ* **2009**, *696*, 1871–1885, [arXiv:astro-ph/0811.1044]. doi:10.1088/0004-637X/696/2/1871.
121. Jin, Z.P.; Hotokezaka, K.; Li, X.; Tanaka, M.; D'Avanzo, P.; Fan, Y.Z.; Covino, S.; Wei, D.M.; Piran, T. The Macronova in GRB 050709 and the GRB-macronova connection. *Nature Communications* **2016**, *7*, 12898, [arXiv:astro-ph.HE/1603.07869]. doi:10.1038/ncomms12898.
122. Troja, E.; Ryan, G.; Piro, L.; van Eerten, H.; Cenko, S.B.; Yoon, Y.; Lee, S.K.; Im, M.; Sakamoto, T.; Gatkine, P.; et al. A luminous blue kilonova and an off-axis jet from a compact binary merger at z = 0.1341. *Nature Communications* **2018**, *9*, [arXiv:astro-ph.HE/1806.10624]. doi:10.1038/s41467-018-06558-7.
123. Kasliwal, M.M.; Korobkin, O.; Lau, R.M.; Wollaeger, R.; Fryer, C.L. Infrared Emission from Kilonovae: The Case of the Nearby Short Hard Burst GRB 160821B. *ApJ* **2017**, *843*, L34, [arXiv:astro-ph.HE/1706.04647]. doi:10.3847/2041-8213/aa799d.
124. Jin, Z.P.; Li, X.; Wang, H.; Wang, Y.Z.; He, H.N.; Yuan, Q.; Zhang, F.W.; Zou, Y.C.; Fan, Y.Z.; Wei, D.M. Short GRBs: Opening Angles, Local Neutron Star Merger Rate, and Off-axis Events for GRB/GW Association. *ApJ* **2018**, *857*, 128, [arXiv:astro-ph.HE/1708.07008]. doi:10.3847/1538-4357/aab76d.
125. Lamb, G.P.; Tanvir, N.R.; Levan, A.J.; de Ugarte Postigo, A.; Kawaguchi, K.; Corsi, A.; Evans, P.A.; Gompertz, B.; Malesani, D.B.; Page, K.L.; et al. Short GRB 160821B: A Reverse Shock, a Refreshed Shock, and a Well-sampled Kilonova. *ApJ* **2019**, *883*, 48, [arXiv:astro-ph.HE/1905.02159]. doi:10.3847/1538-4357/ab38bb.
126. Troja, E.; Castro-Tirado, A.J.; Becerra González, J.; Hu, Y.; Ryan, G.S.; Cenko, S.B.; Ricci, R.; Novara, G.; Sánchez-Rámirez, R.; Acosta-Pulido, J.A.; et al. The afterglow and kilonova of the short GRB 160821B. *MNRAS* **2019**, *489*, 2104–2116, [arXiv:astro-ph.HE/1905.01290]. doi:10.1093/mnras/stz2255.
127. Fong, W.; Laskar, T.; Rastinejad, J.; Escorial, A.R.; Schroeder, G.; Barnes, J.; Kilpatrick, C.D.; Paterson, K.; Berger, E.; Metzger, B.D.; et al. The Broadband Counterpart of the Short GRB 200522A at z = 0.5536: A Luminous Kilonova or a Collimated Outflow with a Reverse Shock? *ApJ* **2021**, *906*, 127, [arXiv:astro-ph.HE/2008.08593]. doi:10.3847/1538-4357/abc74a.
128. Xu, D.; Starling, R.L.C.; Fynbo, J.P.U.; Sollerman, J.; Yost, S.; Watson, D.; Foley, S.; O'Brien, P.T.; Hjorth, J. In Search of Progenitors for Supernovaless Gamma-Ray Bursts 060505 and 060614: Re-examination of Their Afterglows. *ApJ* **2009**, *696*, 971–979, [arXiv:astro-ph/0812.0979]. doi:10.1088/0004-637X/696/1/971.
129. Price, P.A.; Berger, E.; Fox, D.B. GRB 060614: redshift. *GRB Coordinates Network* **2006**, *5275*, 1.
130. Fugazza, D.; Malesani, D.; Romano, P.; Tagliaferri, G.; Covino, S.; Chincarini, G.; Della Valle, M.; Fiore, F.; Stella, L. GRB 060614: redshift confirmation. *GRB Coordinates Network* **2006**, *5276*, 1.

131. Della Valle, M.; Chincarini, G.; Panagia, N.; Tagliaferri, G.; Malesani, D.; Testa, V.; Fugazza, D.; Campana, S.; Covino, S.; Mangano, V.; et al. An enigmatic long-lasting γ-ray burst not accompanied by a bright supernova. *Nature* **2006**, *444*, 1050–1052, [arXiv:astro-ph/astro-ph/0608322]. doi:10.1038/nature05374.
132. Fynbo, J.P.U.; Watson, D.; Thöne, C.C.; Sollerman, J.; Bloom, J.S.; Davis, T.M.; Hjorth, J.; Jakobsson, P.; Jørgensen, U.G.; Graham, J.F.; et al. No supernovae associated with two long-duration γ-ray bursts. *Nature* **2006**, *444*, 1047–1049, [arXiv:astro-ph/astro-ph/0608313]. doi:10.1038/nature05375.
133. Gal-Yam, A.; Fox, D.B.; Price, P.A.; Ofek, E.O.; Davis, M.R.; Leonard, D.C.; Soderberg, A.M.; Schmidt, B.P.; Lewis, K.M.; Peterson, B.A.; et al. A novel explosive process is required for the γ-ray burst GRB 060614. *Nature* **2006**, *444*, 1053–1055, [arXiv:astro-ph/astro-ph/0608257]. doi:10.1038/nature05373.
134. Gehrels, N.; Norris, J.P.; Barthelmy, S.D.; Granot, J.; Kaneko, Y.; Kouveliotou, C.; Markwardt, C.B.; Mészáros, P.; Nakar, E.; Nousek, J.A.; et al. A new γ-ray burst classification scheme from GRB060614. *Nature* **2006**, *444*, 1044–1046, [arXiv:astro-ph/astro-ph/0610635]. doi:10.1038/nature05376.
135. Lu, Y.; Huang, Y.F.; Zhang, S.N. A Tidal Disruption Model for the Gamma-Ray Burst of GRB 060614. *ApJ* **2008**, *684*, 1330–1335, [arXiv:astro-ph/0801.2419]. doi:10.1086/590899.
136. Meng, Y.Z.; Geng, J.J.; Zhang, B.B.; Wei, J.J.; Xiao, D.; Liu, L.D.; Gao, H.; Wu, X.F.; Liang, E.W.; Huang, Y.F.; et al. The Origin of the Prompt Emission for Short GRB 170817A: Photosphere Emission or Synchrotron Emission? *ApJ* **2018**, *860*, 72, [arXiv:astro-ph.HE/1801.01410]. doi:10.3847/1538-4357/aac2d9.
137. Li, L.; Ryde, F.; Pe'er, A.; Yu, H.F.; Acuner, Z. Bayesian Time-Resolved Spectroscopy of Multi-Pulsed GRBs: Variations of Emission Properties amongst Pulses. *arXiv e-prints* **2020**, p. arXiv:2012.03038, [arXiv:astro-ph.HE/2012.03038].
138. Dereli-Bégué, H.; Pe'er, A.; Ryde, F. Classification of Photospheric Emission in Short GRBs. *ApJ* **2020**, *897*, 145, [arXiv:astro-ph.HE/2002.06408]. doi:10.3847/1538-4357/ab9a2d.
139. Li, L. Multipulse Fermi Gamma-Ray Bursts. I. Evidence of the Transition from Fireball to Poynting-flux-dominated Outflow. *ApJS* **2019**, *242*, 16, [arXiv:astro-ph.HE/1810.03129]. doi:10.3847/1538-4365/ab1b78.
140. Acuner, Z.; Ryde, F.; Pe'er, A.; Mortlock, D.; Ahlgren, B. The Fraction of Gamma-Ray Bursts with an Observed Photospheric Emission Episode. *ApJ* **2020**, *893*, 128, [arXiv:astro-ph.HE/2003.06223]. doi:10.3847/1538-4357/ab80c7.
141. Acuner, Z.; Ryde, F. Clustering of gamma-ray burst types in the Fermi GBM catalogue: indications of photosphere and synchrotron emissions during the prompt phase. *MNRAS* **2018**, *475*, 1708–1724, [arXiv:astro-ph.HE/1712.01568]. doi:10.1093/mnras/stx3106.
142. Ryde, F. The Cooling Behavior of Thermal Pulses in Gamma-Ray Bursts. *ApJ* **2004**, *614*, 827–846, [arXiv:astro-ph/astro-ph/0406674]. doi:10.1086/423782.
143. McBreen, S.; McBreen, B.; Hanlon, L.; Quilligan, F. Cumulative light curves of gamma-ray bursts and relaxation systems. *A&A* **2002**, *393*, L29–L32, [arXiv:astro-ph/astro-ph/0208347]. doi:10.1051/0004-6361:20021073.
144. Abbott, B.P.; Abbott, R.; Abbott, T.D.; Abraham, S.; Acernese, F.; Ackley, K.; Adams, C.; Adya, V.B.; Affeldt, C.; Agathos, M.; et al. Prospects for observing and localizing gravitational-wave transients with Advanced LIGO, Advanced Virgo and KAGRA. *Living Reviews in Relativity* **2020**, *23*, 3. doi:10.1007/s41114-020-00026-9.
145. Ivezić, Ž.; Kahn, S.M.; Tyson, J.A.; Abel, B.; Acosta, E.; Allsman, R.; Alonso, D.; AlSayyad, Y.; Anderson, S.F.; Andrew, J.; et al. LSST: From Science Drivers to Reference Design and Anticipated Data Products. *ApJ* **2019**, *873*, 111, [arXiv:astro-ph/0805.2366]. doi:10.3847/1538-4357/ab042c.
146. Harris, C.R.; Millman, K.J.; van der Walt, S.J.; Gommers, R.; Virtanen, P.; Cournapeau, D.; Wieser, E.; Taylor, J.; Berg, S.; Smith, N.J.; et al. Array programming with NumPy. *Nature* **2020**, *585*, 357–362. doi:10.1038/s41586-020-2649-2.
147. Hunter, J.D. Matplotlib: A 2D graphics environment. *Computing in Science & Engineering* **2007**, *9*, 90–95. doi:10.1109/MCSE.2007.55.
148. pandas development team, T. pandas-dev/pandas: Pandas, 2020. doi:10.5281/zenodo.3509134.
149. Wes McKinney. Data Structures for Statistical Computing in Python. Proceedings of the 9th Python in Science Conference; Stéfan van der Walt.; Jarrod Millman., Eds. SciPy (Austin, TX, USA), 2010, pp. 56 – 61. doi:10.25080/Majora-92bf1922-00a.
150. Pedregosa, F.; Varoquaux, G.; Gramfort, A.; Michel, V.; Thirion, B.; Grisel, O.; Blondel, M.; Prettenhofer, P.; Weiss, R.; Dubourg, V.; et al. Scikit-learn: Machine Learning in Python. *Journal of Machine Learning Research* **2011**, *12*, 2825–2830.